TÜBİTAK

Turkish Journal of Earth Sciences

http://journals.tubitak.gov.tr/earth/

Research Article

Turkish J Earth Sci
(2020) 29: 831-852
© TÜBİTAK
doi:10.3906/yer-2002-9

Nature of clays in Late Cretaceous dacitic rocks in the eastern Sakarya Zone (NE Turkey): a geochemical and isotopic approach

Ferkan SİPAHİ[1,*], Mehmet Ali GÜCER[1], Münür Burhan SADIKLAR[2]

[1]Department of Geological Engineering, Faculty of Engineering and Natural Sciences, Gümüşhane University, Gümüşhane, Turkey
[2]Department of Geological Engineering, Faculty of Engineering, Karadeniz Technical University, Trabzon, Turkey

Received: 13.02.2020 • **Accepted/Published Online:** 21.06.2020 • **Final Version:** 04.09.2020

Abstract: Late Cretaceous felsic rocks are common in the eastern Pontides (NE Turkey). These rocks developed as an island arc from the Jurassic to the Miocene; they also host numerous volcanogenic massive sulfide deposits. The Late Cretaceous dacites that outcrop around Zigana Mountain (Gümüşhane, NE Turkey) were exposed to intensive hydrothermal alteration. Widespread hydrothermal alteration of Late Cretaceous dacite in Zigana Mountain has led to the formation of well-developed clay minerals. Their main alteration products are sericite, chlorite, and carbonates (ankerite and calcite). The clay minerals identified by X-ray diffraction and differential thermal analysis include illite, chlorite, small amounts of kaolinite, and smectite. The polytype of illite is $2M_1$. Illites formed as a result of hydrothermal alteration of feldspars; they are also Fe- and Mg-poor. Chlorite is characterized by decreasing Fe/(Fe+ Mg) ratio with increasing alteration grade and has a trioctahedral structure. Chlorite geothermometer calculations (100–300°C) reflect the activities of hydrothermal solutions. Chlorite forms in more alkaline conditions compared with illite, as its formation is associated with the presence of carbonates. Oxygen and hydrogen stable isotope values, K-Ar dating of illites, and textural and chemical evidence suggest that clays might have formed mainly by alteration of minerals in dacitic rocks with hydrothermal fluids of magmatic origin during the Campanian under acidic–weak alkaline conditions.

Key words: Clay minerals, Late Cretaceous altered dacites, hydrothermal alteration, K-Ar dating, eastern Pontides (NE Turkey)

1. Introduction

The study area is located in the eastern part of the Sakarya Zone called the eastern Pontide (Black Sea Region), North Turkey. It is formed of rocks from the Late Cretaceous epoch, such as those in the metallogenic province in the eastern part of the Black Sea region (Figure 1; Table 1). This eastern Black Sea (Pontide) metallogenic province lies along an E–W line in the region and developed as an island arc from the Jurassic to the Miocene during the subduction of the Tethyan oceanic crust under the Sakarya Zone (Şengör and Yılmaz, 1981). Volcanic activity in the Pontides began during the Liassic. Basic rock formation during this period occurred in a rift environment, which developed on a Precambrian to Paleozoic basement (Schnieder et al., 1988; Arslan et al., 1997), forming volcanic rocks that are predominantly felsic. Felsic rocks are followed in an upward sequence by Late Cretaceous to Eocene volcanic and granitoid rocks. Intensively altered, they host numerous massive sulfide, vein type, skarn and clay deposits (Altun, 1972; Buser and Cvetic, 1973; Nebioğlu, 1975; Pejatoviç, 1979; Çağatay, 1993; Özgür, 1993; Tüysüz, 2000; Sipahi, 2011; Karakaya et al., 2011a, 2011b; Akaryalı and Tüysüz,2013; Sipahi et al., 2014, 2017, 2020; Akyürek and Sipahi, 2014; Karakaya et al., 2015; Akaryalı, 2016; Akaryalı and Akbulut, 2016). In the eastern Pontide, volcanogenic massive sulfide (VMS) deposits were emplaced in the intra-arc rift zone of the magmatic island arc (Turkey), which is characterized by bimodal volcanic rocks and hosted by the Late Cretaceous dacites (Çağatay, 1993; Çiftçi and Hagni, 2005; Çiftçi et al., 2005; Abdioğlu and Arslan, 2008; Karakaya et al., 2012; Sipahi and Sadıklar, 2010, 2014; Sipahi et al., 2014; Eyüboğlu et al., 2014; Abdioğlu et al., 2015; Sipahi, 2017). Mineralogical and geochemical studies in the Kutlular (Trabzon, Turkey) massive sulfide deposit show that the alteration zones are represented by silicification-pyrite-illite, illite-silicification, illite/smectite-silicification, smectite zone accompanying kaolinite and halloysite in the dacitic pyroclastics, and chlorite in the mafic volcanics (Abdioğlu and Arslan, 2008). Illite, kaolinite, chlorite, smectite, and lower amounts of interlayered illite/smectite were determined as clay minerals in the Kıbletepe (Trabzon, Turkey) massive

* Correspondence: ferkansipahi@gmail.com

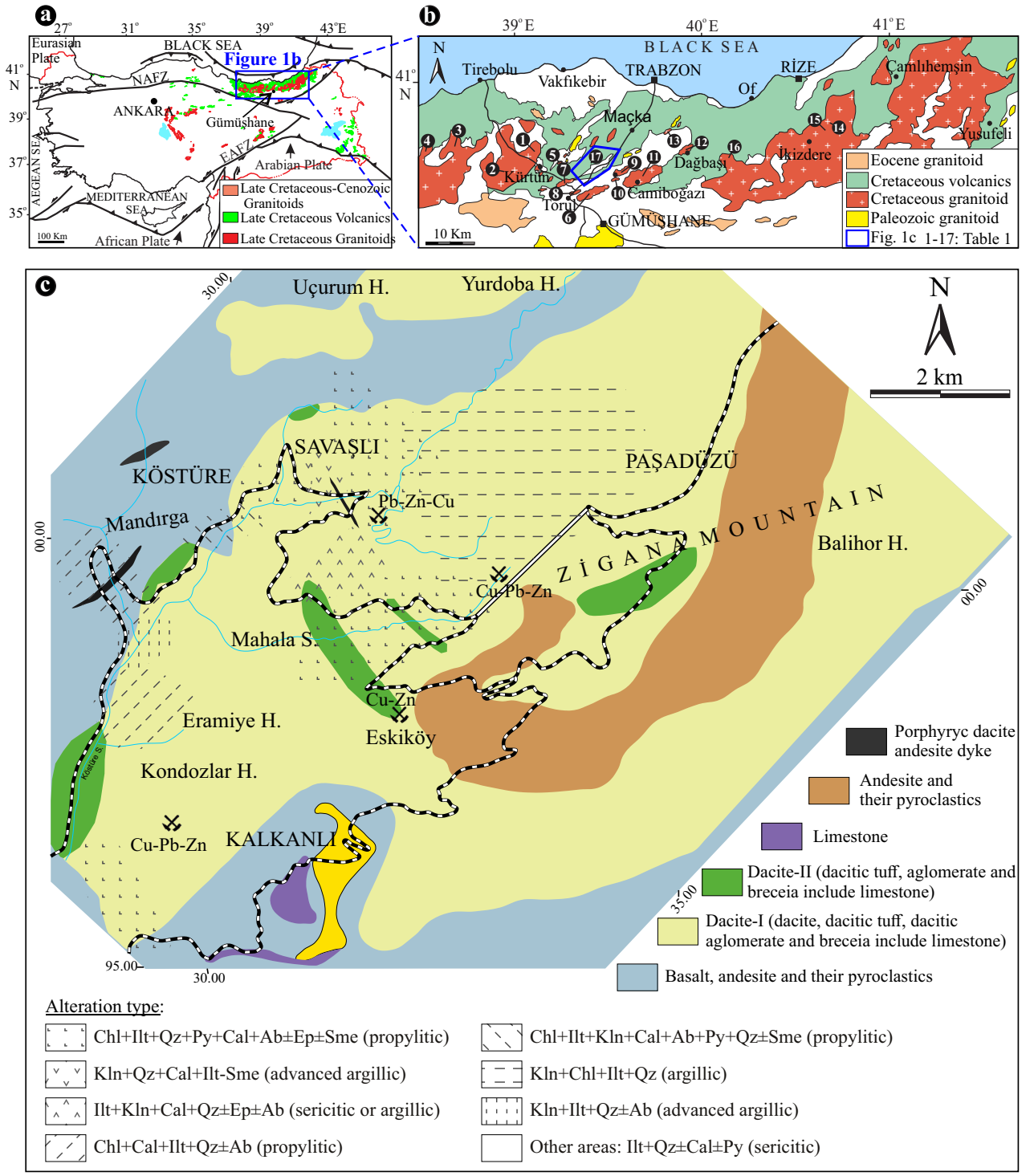

Figure 1. (a) Late Cretaceous magmatic rocks of NE Turkey (modified after MTA, 2011), and (b) simplified geological map showing the granitoid distribution in the eastern Pontides (modified after Gedik et al., 1992; geochronological data (1–17) is given in Table 1). NAFZ: North-Anatolian fault zone; EAFZ: East-Anatolian fault zone. (c) Geological and alteration map of the Zigana Mountain, NE Turkey.

sulfide mineralization (Akyürek and Sipahi, 2014). Mineralogical studies in the Murgul (Artvin, Turkey) massive sulfide deposit indicate the presence of illite, illite/smectite + chlorite ± kaolinite and chlorite in the footwall rock and illite ± smectite ± kaolinite and chlorite ± illite in the hanging wall rock (Abdioğlu et al., 2015).

Table 1. The geochronological data of Late Cretaceous magmatic rocks from the eastern Pontides (NE Turkey).

Locations in Figure 1b	Magmatic rock	Age (Ma)	Method	References
1-Harşit	Q-monzonite	79	Ar-Ar	Karslı et al. (2010)
2-Kürtün	Granodiorite	68	K/Ar	Jica (1986)
3-South of Dereli	Granodiorite	69–74	Fission track (apatite)	Boztuğ et al. (2004)
4- East of Dereli	Granodiorite	71–84	K/Ar	Moore et al. (1980)
5-Arpaköy	Diorite	82	U-Pb (zircon)	Kaygusuz et al. (2012b)
6-Torul	Granitoid	78–80	U-Pb (zircon)	Kaygusuz et al. (2010)
7-Sarıosman	Monzogranite	82	U-Pb (zircon)	Kaygusuz et al. (2009)
8-Köprübaşı	Granodiorite	79	U-Pb (zircon)	Kaygusuz and Şen (2011)
9-Turnagöl	Granodiorite	78	U-Pb (zircon)	Kaygusuz et al. (2013)
10-Ayeser	Q-monzonite	74	U-Pb (zircon)	Kaygusuz et al. (2012b)
11-Camiboğazı	Granitoid	72–76	U-Pb (zircon)	Kaygusuz et al. (2014)
12-Dağbaşı	Granitoid	83–88	U-Pb (zircon)	Kaygusuz and Aydınçakır (2011)
13-Oyman	Granite	86	U-Pb (zircon)	Kaygusuz et al. (2012b)
14-İkizdere	Granodiorite	79	K/Ar	Moore et al. (1980)
15-İkizdere	Granodiorite	70–80	K/Ar	Taner (1977)
16-Araklı	Granodiorite	75	K/Ar	Yılmaz-Şahin (2005)
17-Zigana	Dacite-I	77–82	K/Ar (illite)	This study
	Dacite-II	73–78	K/Ar (illite)	This study

Some of the Late Cretaceous dacitic rocks were studied to determine the alteration mineralogy and chemistry of wall rocks (e.g., Çelik et al., 1999; Tüysüz, 2000; Karakaya and Karakaya, 2001a, 2001b; Karakaya et al., 2007; Sipahi and Sadıklar, 2010; Akyürek and Sipahi, 2014). Widespread and intense hydrothermal alteration zones in the Cretaceous Şaplıca volcanics (Giresun, Turkey) include propylitic, phyllitic (quartz-sericite, pyrite-sericite), and argillic types of alteration, along with hematite, silica polymorphs, and two different types of tourmaline mineralization (Karakaya et al., 2007).

Dacitic rocks around Zigana Mountain (Gümüşhane, NE Turkey) show intensive hydrothermal alteration and minimal weathering. Only a few observations were made about the alteration (e.g., Güven, 1993), as no comprehensive studies about the alteration of mineralogy, chemistry, and formation have been carried out so far. Thus, the main objective of this study is to investigate the mineral chemistry, stable isotopes, and properties of the formation environment of clay minerals that are widespread and resulted from hydrothermal alteration of Late Cretaceous dacitic rocks in the Zigana Region.

2. Geological setting and local geology

The eastern Pontides are the result of three main Neo-Tethyan volcanic cycles during Eocene, upper Cretaceous, and Jurassic times (Kazmin et al., 1986). These three volcanic cycles represent arc volcanism and plutonism to post-subduction alkaline volcanism, and paleo-island arc and long-term crustal evolution from pre-subduction rifting (Şengör and Yılmaz, 1981). There are three different geological zones present in the eastern Pontides based on lithological characteristics: the northern, southern, and axial zones. The southern zone mostly contains Paleozoic metamorphic and plutonic rocks and their sedimentary series, whereas the northern zone is characterized by extensive Upper Cretaceous and Tertiary volcanic rocks cropping out mainly along the Black Sea coast (Arslan et al., 1997; Topuz et al., 2007). The axial zone is mostly characterized by upper mantle peridotite and Middle to Upper Cretaceous olistostromal mélange. Volcanic activity in the Pontides began during the Liassic, with the formation of basic rocks in a rift environment, which developed on a Precambrian to Paleozoic basement (Okay and Şahintürk, 1997; Arslan et al., 1997; Topuz et al., 2010; Dokuz, 2011; Kaygusuz et al., 2012, 2016).The volcanic rocks are dominantly felsic, and they are overlain by Late Cretaceous to Eocene volcanic rocks (Bektaş et al., 1999). The Late Cretaceous volcanic rocks are tholeiitic to calc-alkaline in composition. These volcanics consist of rhyolite, dacite and minor basalt, andesite, and their pyroclastic equivalents.

The basement of the study area comprises mostly Late Cretaceous volcanics, formed by Late Cretaceous basalt,

andesite, and respective pyroclastics. The basement is further covered by Late Cretaceous dacitic rocks (i.e. dacite-I and dacite-II), as described by Sipahi (2005) and Sipahi and Sadıklar (2014). These latter rocks are made up of lavas, agglomerates, and tuffs, and are conformably overlain by andesite and pyroclastics. Macroscopically, the basalt and andesite are dark green, green, blackish, and brownish. Basalt and andesite generally contain fractures, visible feldspar phenocrysts, and rock fragments of variable sizes. The dacites (dacite-I and dacite-II) from Zigana have similar mineralogy and features and are generally fractured and altered (Figures 2a and 2b). They range from white, yellow, pink, yellowish-white, to greenish-white, and show occasional prismatic structures. The dacitic agglomerates contain disseminated pyrite with sizes ranging from 0.2 mm to 1 cm. The top of the andesite is dark green and brownish and is generally fractured. All volcanic rocks, except for the top of the andesite, include locally gray and red limestone lenses with a thickness of ~1–3 m. The age of the volcanics corresponds to the Late Cretaceous (Turonian to Santonian) based on paleontological evidence (*Marginotruncana pseudolinneiana*, *Marginotruncana sp.*, *Globigerinelloides sp.*, *Dicarinella sp.*,and*Ticinella sp.*; Sipahi, 2005). The youngest units are andesitic and porphyric dacitic dykes, which are dark green and white-colored, respectively (Sipahi et al., 2019). Porphyritic dacitic dykes have mega-quartz crystals. All volcanics are hydrothermally overprinted.

3. Analytical methods

3.1. SEM-EDS and EPMA analysis

Micromorphological and textural features of various clays from broken rock fragments were examined by coating them with gold using a Zeiss DSM 960 A scanning electron microscope (SEM) (Freie University, Berlin, Germany). The EDAX ZAF Quantification Element Normalized program was employed for analysis with SEM-energy dispersive spectroscopy (EDS) (Freie University, Berlin, Germany).

Thin sections from altered dacites were carbon-coated and analyzed with a CAMECA SX-100 wavelength-dispersive electron microprobe (Institute of Mineralogy and Petrology of Hamburg University, Hamburg, Germany). The instrument was operated at an acceleration voltage of 15–20 kV and a beam current of 20 nA; its beam diameter was less than 1 μm.

3.2. X-ray diffraction (XRD) analysis

Eighty samples were collected from the dacitic rocks on Zigana Mountain (Gümüşhane, NE Turkey). From these, 49 samples were chosen for X-ray diffraction (XRD) in whole rock and clay fraction studies. Whole-rock samples selected for XRD were ground using agate mortar and pestle. Approximately 20–30 g of this material were chemically treated (Jackson, 1956; Gündoğdu and Yılmaz, 1984) with 1 N acetic acid in order to extract the carbonates. The sodium dithionite-citrate procedure was applied to remove free Fe-oxides (Jackson, 1956; Mehra and Jackson, 1960; Kunze, 1965). Clay fractions (<2 μm) were separated by sedimentation, followed by standard centrifugation techniques(Schroeder, 2018). XRD analyses were carried out using a Rigaku DMAX 3C model XRD (Physics Department of Karadeniz Technical University, Trabzon, Turkey) and Philips PW1710 model XRD (Cu Ka and Ni filter, 18 and 30 mA, 40 kV, speed 1°/min; Freie University Berlin, Germany). The samples were scanned in the range 3–35 °2θ using a 0.02 °2θ step. Oriented clay fractions were analyzed in the untreated state (N) after saturation with ethylene glycol (EG: 60°C for 16 h) and heating (H: 490°C for 4 h).

3.3. Differential thermal analysis (DTA)

Differential thermal analysis (DTA) of the <2 μm fractions was conducted using a NETZCH 404 differential thermal instrument under air at Karadeniz Technical University (Trabzon, Turkey). Pressed powder samples were heated to 1100 °C at a rate of 5 °C/min. Al_2O_3 was used as a reference.

3.4. K-Ar age analysis

Six samples containing pure illite, chosen from Zigana dacites, were analyzed at the Actlabs Laboratories Ltd. (Ancaster, ON, Canada) for K-Ar age. For Ar analysis, argon concentration was determined using isotope dilution with ^{38}Ar spike; these were introduced to the sample system prior to individual extraction. Then, pure Ar was introduced onto the custom-built magnetic sector mass spectrometer (Reinolds type) with a Varian CH5 magnet. The measurement of Ar isotope ratios was corrected for mass discrimination. Atmospheric argon was removed, assuming that only air contributed to ^{36}Ar. The concentration of radiogenic ^{40}Ar was calculated with ^{38}Ar spike concentration. For K-analysis, the aliquot of the sample was weighed on a graphite crucible with lithium metaborate/tetraborate flux and fused using a LECO induction furnace. The standards, blanks, and sample were analyzed using Thermo Jarrell Ash Enviro II ICP spectrometer.

3.5. O and H isotope analysis

Six extracted illite samples were analyzed for oxygen and hydrogen stable isotopes at the Actlabs Laboratories (Canada). The oxygen extraction technique was based on BrF_5 digestion at ~650°C in nickel bombs following the procedures described by Clayton and Mayeda (1963). Isotopic analyses were performed with Finnigan MAT Delta, dual inlet, and isotope ratio mass spectrometer. The data are presented as standard delta notation [$\delta^{18}O = (^{18}O/^{16}O_{sample}/^{18}O/^{16}O_{VSMOW} - 1)10^3$] in accordance with mil deviations from V-SMOW. External reproducibility was ±0.19‰ (1σ) based on the repeat analyses of the

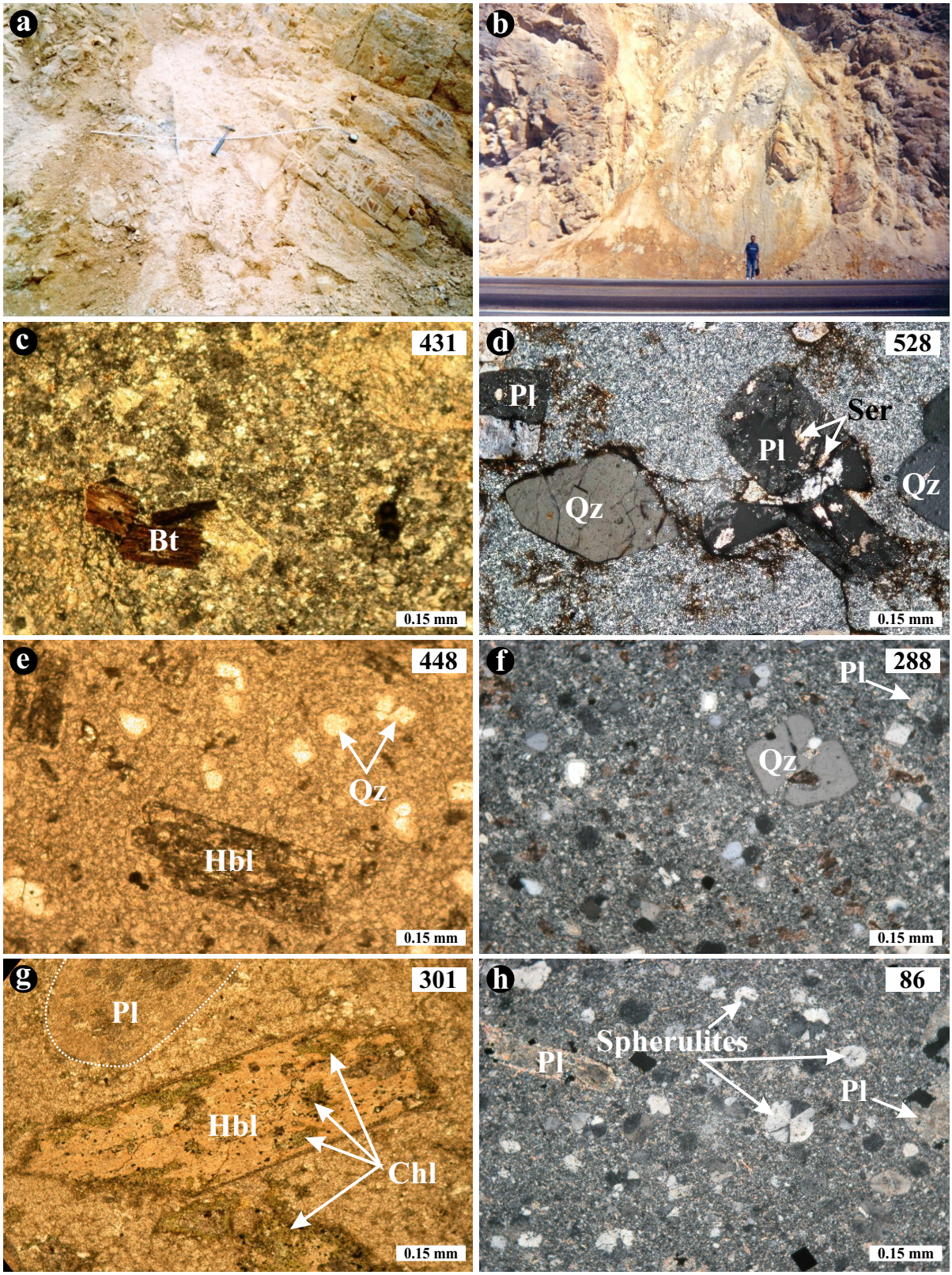

Figure 2. Field and photomicrographs of the dacites. a) and b) altereddacite; c)twisted biotite (dacite-II); d)quartz and plagioclase (dacite-I); e) and g) altered hornblende (sample 448 from dacite-I and sample 301 from dacite-II, //N); f) and h) spherulitic texture (sample 288 from dacite-I and sample 86 fromdacite-II, +N). Qz: Quartz; Pl: Plagioclase; Hbl: Hornblende; Chl: Chlorite; Ser: Sericite.

internal white crystal standard (WCS) of Actlabs. The value of NBS 28 was 9.61 ±0.10‰ (1σ). Analyses of water content were reproducible to ±0.2 wt%. Isotopic analyses via conventional isotope ratio mass spectrometry are presented in the familiar notation as per mil relative to V-SMOW standard. Duplicate analyses were performed on a number of samples. The δD values agreed well with ±3; δD value was measured as–65 in relation to the NSB–30 biotite standard.

4. Results

4.1. Field relations and petrographic observations of dacites

The two series of dacitic rocks are composed of lavas, agglomerates, and tuffs. They exhibit porphyritic, less spherulitic, and glomerophyric textures (Figures 2c–2h). Petrographically, the dacites present similar textural features and mineral compositions. The rocks contain phenocrystals of mainly quartz, plagioclase, amphibole (hornblende), sanidine, biotite, and muscovite. Zircon and rutile were accessory minerals. Quartz appears as euhedral and subhedral microcrysts and phenocrysts (Figures 2c–2h). Plagioclase micro- and phenol-crystals are partly sericitized and argilized (Figures 2c–2h). Hornblendes are intensely fractured, occasionally chloritized, carbonatized, and silicified, as well as lined by opaque rims (Figure 2g). Some biotite minerals are chloritized and exhibit deformation textures from the compaction of the rocks. Pyroclastic rocks are found with agglomerates, lithic-crystal tuffs, and crystal tuffs (Schmid, 1981), and mainly with plagioclase, primary and secondary quartz, and disseminated opaque minerals (pyrite and hematite, and some chalcopyrite and covellite). The rock fragments present a dacitic composition. Secondary minerals are represented by sericite (illite), chlorite, kaolinite, smectite, and carbonate minerals (calcite and ankerite) as alteration products of the primary minerals in the dacitic rocks. Clay minerals dominate the alteration products of feldspar, biotite and muscovite, and chlorite for the ferromagnesian minerals (hornblende and biotite).

Evidently, dacitic rocks were affected by the tectonic activity in the region. The fault system controlled the emplacement of various alteration zones. The tectonic structure of the region was determined by N 20–70° W and N 20–70° E strikes. Based on volcanic fracture measurements, the N 40–50° W and N 60–70° E strikes for fractures were appropriately represented in lithologic units and showed specific importance in terms of ore setting directions (Gümüş, 1998).

4.2. Clay mineralogy

Semiquantitative analysis of clay minerals, such as illite, chlorite, kaolinite, and smectite was performed by XRD (Table S1; Figure3). Illite was the most abundant clay mineral in dacitic rocks, followed by chlorite. The other constituents of the <2 μm fraction samples were very low and rare, consisting of feldspar, quartz, kaolinite, and smectite. Studies generally indicate that illite is the most common alteration product.

Based on clay mineralogy, hydrothermal alteration assemblages might represent illite-chlorite-silica (propylitic) zone and illite-silica (sericitic) zone that accompany the kaolinite in the dacitic rocks.

The DTA of some samples, including the clay of <2 μm fraction, showed three major endothermic events attributed to illite and kaolinite (Figures 4a and 4b). The first low temperature endothermic event at about 100–155°C was due to a loss of adsorbed water. The second event at about 560°C reflected dehydroxylation (loss of the hydroxyl water). The third endotherm was observed at ~890°C.

Scanning electronic microscope (SEM) images revealed the morphologies of illite and kaolinite. The rims of some illites were well defined, others formed long crystals (Figures 5a and 5b), whereas some illite crystals were subhedral (Figures 5c and 5d). The length of the illite crystals varied from 5 to 15 μm. Stacked particles were common (Figure5b). The shape of the accompanying kaolinite stack (Figure5e) was significant and formed books. The kaolinite booklet stack is a characteristic feature of hydrothermal kaolinite (Keller, 1976).

4.3. Mineral chemistry of the clay minerals

The K_2O content of illites was 7.99–8.88 wt% (average 8.27 wt%) in dacite-I and 7.90–8.88 wt% (average 8.57 wt%) in dacite-II. The K and Na interlayer occupancy was 0.66–0.78 atoms and 0.02–0.20 atoms per unit formula, respectively, in dacite-I, and 0.66–0.75 atoms and 0.02–0.05 atoms, respectively, for dacite-II (Table 2). The negative charge in octahedral and tetrahedral structures was balanced by the interlayer charge. When the compositions of the illites were plotted on the (Fe+Mg)-K-Si (Figure6a) and MR^3-$2R^3$-$3R^2$ (Figure6b) ternary diagrams, the illites in dacite-I were richer in Fe + Mg compared to their counterparts from dacite-II. The octahedral (Fe+Mg) content ranged from 0.30 to 0.41 in dacite-I, and from 0.18 to 0.21 in dacite-II. The Mg content ranged from 0.17–0.30 (dacite-I) and 0.09–0.12 (dacite-II) moles in formula unit, whereas octahedral Al varied from 1.66 to1.72 and 1.82–1.86 in dacite-I and II, respectively. In effect, the illite had low Mg content. The K/Na and K/Mg ratios of illite in dacite-I and II varied between 3.55–36.5 and 2.23–8.11, respectively.

The chlorites were trioctahedral with Fe/(Fe+Mg) ratio varying between 0.28 and 0.45 (average 0.37, Table 3). This ratio provides information about the origin of the chlorite. Chlorite geothermometry was used to determine the formation temperature of the minerals. The method is based on the variation of tetrahedral Al^{3+}

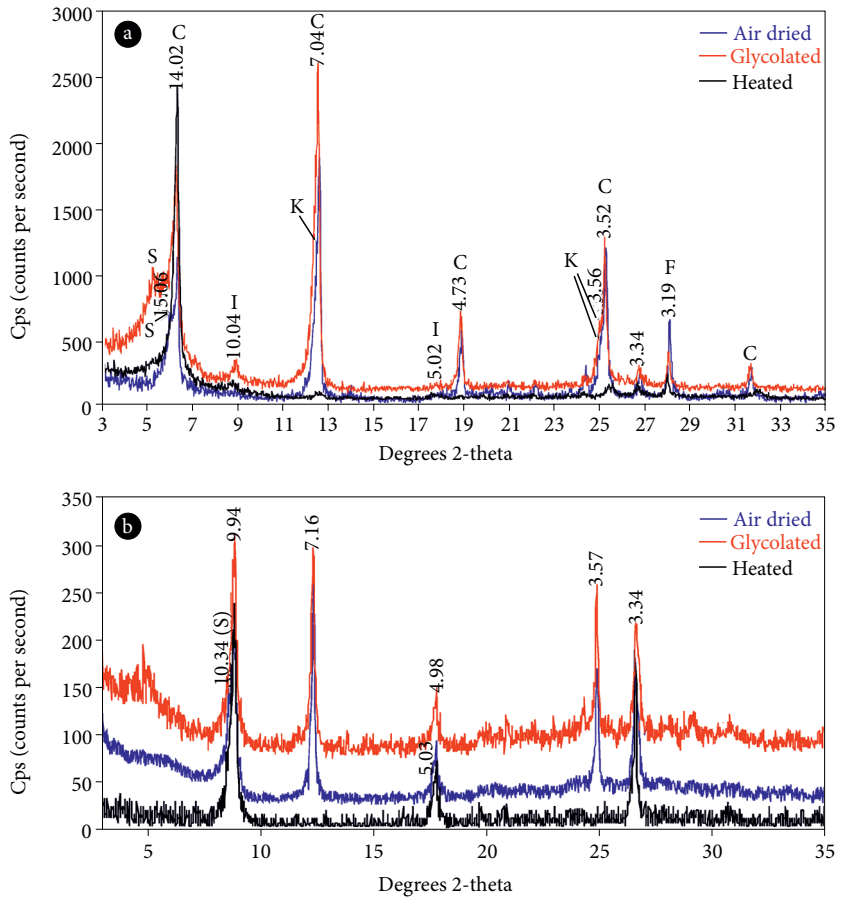

Figure 3. Representative XRD patterns of dacitic rocks from Zigana (NE-Turkey). (a) samples 275a, dacitic tuff; (b) sample 232, illite, chlorite, kaolinite, and smectite minerals. C: Chlorite; I: Illite; K: Kaolinite; S: Smectite.

as a function of temperature (Cathelineau, 1988). The tetrahedral Al content increases with rising temperature. This relationship between Al^{3+} and Si^{4+} in the tetrahedral position, as determined by Cathelineau and Nieva (1985), was modified by Cathelineau (1988) as follows: T (°C) = 321.98 ×Al^{iv}– 61.92. Jowett (1991) subsequently rearranged Cathelineau's (1988) formula using the $Fe^{2+}/(Fe^{2+}+Mg)$ value to reflect the influence of bulk rock composition. The formation temperature of the chlorite in our samples was calculated according to Jowett (1991) using the $Fe^{2+}/(Fe^{2+}+Mg)$ value (Table 4). The temperatures ranged from 110 to 315°C in dacite-I. The temperature reflects the physico-chemical condition of the hydrothermal fluids. This suggests further temperature fluctuation during chlorite formation.

4.4. Whole-rock geochemistry

Except for some trace elements and rare earth elements (REEs), no significant difference was present in petrography and major element composition of the dacites because of extreme hydrothermal and weathering overprinting. The latter data allowed for the separation of the dacites into two different groups of dacite-I and dacite-II (Sipahi, 2005; Sipahi and Sadıklar, 2014; Sipahi et al., 2019). Consequently, in order to establish precursor compositions and chemical affinities of the least altered and hydrothermally altered rocks, high field strength elements (HFSE), namely Ti, Zr, Nb, and Y were used. REE, particularly heavy REE, were also utilized, as they are generally considered immobile in the alteration zones around large numbers of volcanic-hosted massive sulfides and during low-grade metamorphism (MacLean and Kranidiotis, 1987; Elliot-Meadows and Appleyard, 1991; Gemmel and Large, 1992; MacLean and Barret, 1993; Callaghan, 2001). In order to classify Zigana dacites with intense hydrothermal alteration, the immobile element (Zr, Ti, Nb, Yr) chemical discrimination diagram of Winchester and Floyd (1977), and subsequently revised by Pearce (1996), was applied. Both field observations and microscope investigations showed that the dacites were altered to various degrees. Therefore, only the

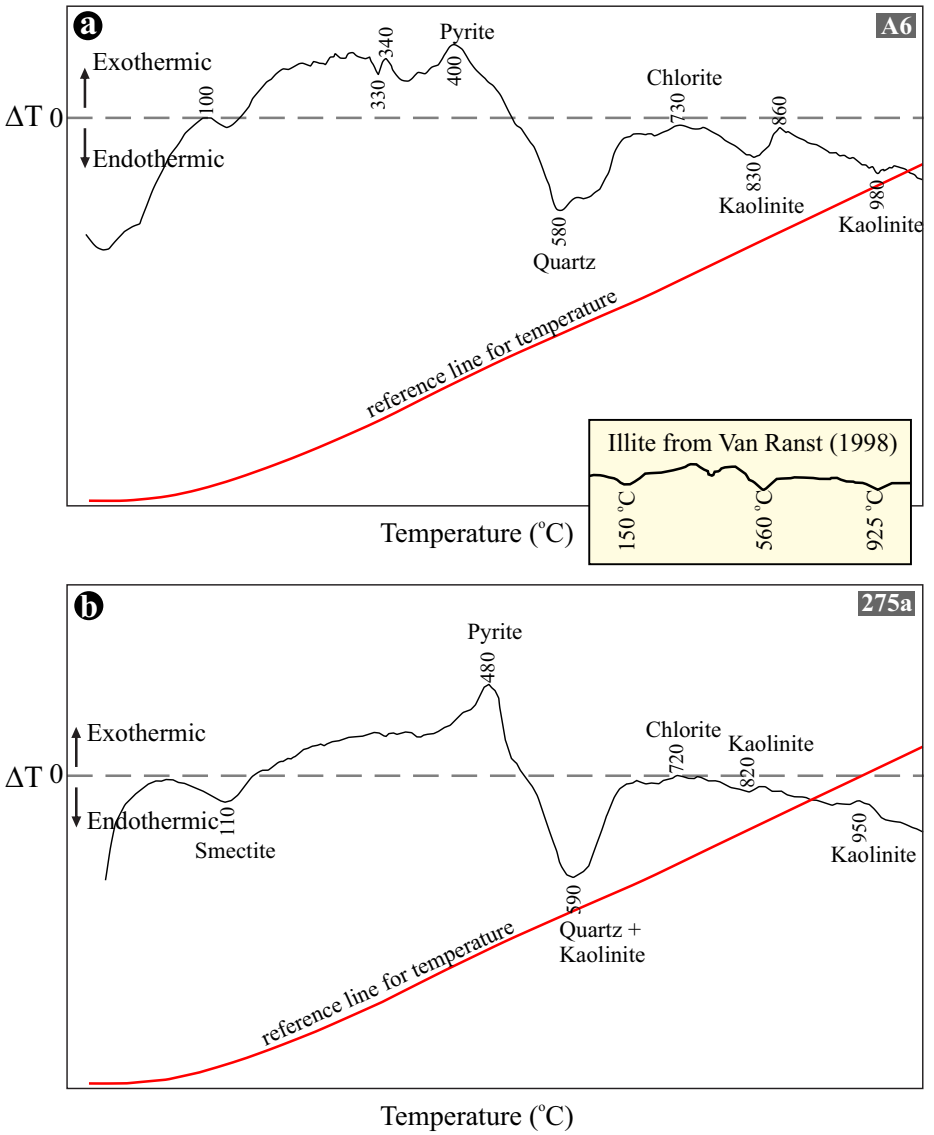

Figure 4. Representative DTA curves of clays from the <2 μm size fraction. (a) Sample of A6 from dacite-I, and (b) sample of 275a from dacite-I. The samples were compared with Van Ranst (1998) illite curves.

immobile element diagram (MacLean and Kranidiotis, 1987; MacLean, 1990; Barret et al., 1993) reduces the effect of alteration on rock classification. Dacites and their pyroclastic equivalents were within the andesite/basaltic andesite field, probably due to slight enrichment of Y and decrease of Zr. However, the mineralogy of dacites showed dacitic composition. In this diagram, Y is slightly more mobile than Nb because of hydrothermal alteration, whereas the Ti element is highly immobile (Barrett and MacLean, 1991; Hill et al., 2000).

4.5. Whole-rock alteration mineralogy

Alteration mineralogy of the dacitic rocks was calculated by using the MINSQ method (Hermann and Berry, 2002) based on whole-rock lithogeochemistry (Table S2). In this method, the present mineral chemistry analyses of dacitic rocks in this study and the literature are used (Deer et al., 1992; Dana, 1993). Quartz, K-feldspar, albite, hornblende, chlorite, ankerite, illite (sericite), calcite, kaolinite, pyrophyllite, hematite, smectite, and epidote were determined in dacite-I (Figure 7a) and quartz, K-feldspar, oligoclase, hornblende, chlorite, muscovite, ankerite, illite, pyrophyllite, kaolinite, pyrite, hematite, calcite, and epidote were estimated in dacite-II (Figure 7b). These constituent minerals estimated from whole-rock lithogeochemistry are consistent with the results of the microscopic analysis and XRD data of the dacite. Illite (6–50 wt%), chlorite (0–11

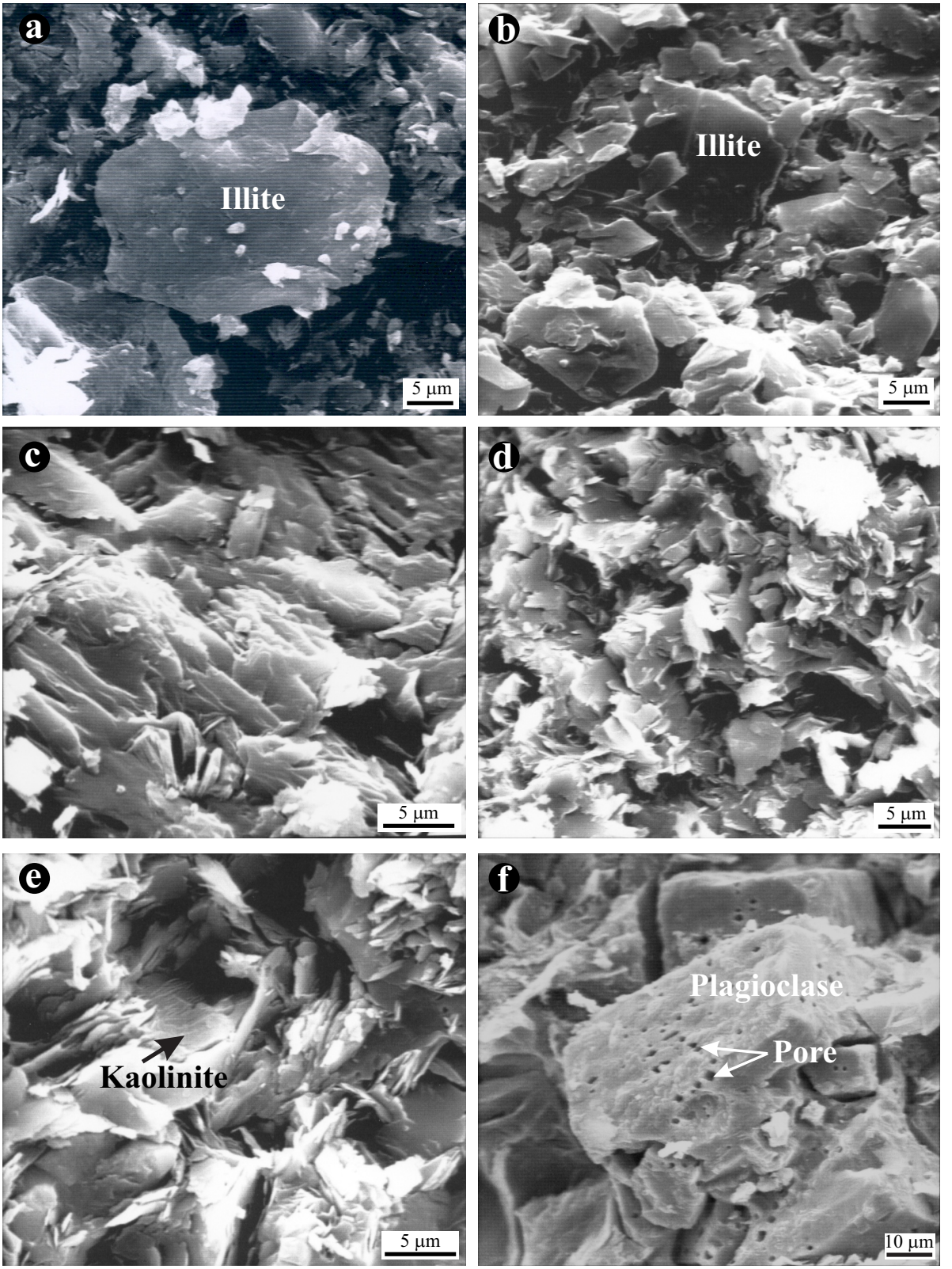

Figure 5. SEM images showing the textural relationship between clays minerals in dacite rock fragments: (a) and (b) illite with well-developed rims (D8 from dacite-I, and 496 from dacite-II); (c) and (d) illite (D8 from dacite-I and 131 from dacite-II); (e) illites surround poorly developed kaolinite (131 from dacite-II); (f) the dissolution cavities in plagioclase (496 from dacite-II).

Table 2. Selected electron microprobe analyses (wt%) of illites in dacite-I and dacite-II, and structural recalculation.

Illite in dacite-I							Illite in dacite-II										
Point	#34	#35	#36	#37	#38	#40	#1	#2	#3	#4	#5	#7	#8	#9	#10	#11	#12
SiO_2	51.46	48.95	51.93	50.37	51.05	52.04	49.73	49.58	49.75	49.45	51.06	48.07	49.63	49.85	49.52	49.63	50.43
TiO_2	0.03	0.04	0.13	0.13	0.04	0.02	0.13	0.13	0.13	0.13	0.08	0.09	0.08	0.10	0.13	0.11	0.08
Al_2O_3	27.51	28.51	29.44	31.28	31.94	30.46	33.30	32.58	33.26	33.04	32.99	31.54	31.53	32.83	32.84	32.80	33.17
FeO*	2.25	1.90	2.02	1.70	2.03	1.20	1.55	1.54	1.50	1.48	1.66	1.75	1.40	1.52	1.47	1.53	1.55
MnO	0.13	0.12	0.10	0.12	0.41	0.15	bdl	bdl	0.01	bdl	0.01	0.03	bdl	0.02	bdl	bdl	0.01
Cr_2O_3	bdl	bdl	0.01	0.04	bdl	0.02	0.016	bdl	bdl	bdl	0.02	0.03	0.04	0.04	bdl	0.06	bdl
NiO	bdl	0.03	0.04	bdl	bdl	0.01	0.04	bdl	0.02	bdl	0.04	bdl	bdl	bdl	bdl	bdl	bdl
MgO	1.72	2.12	3.06	3.06	3.06	2.88	1.24	0.95	1.15	1.18	1.01	1.05	1.13	1.01	1.05	1.06	1.04
CaO	0.09	0.07	0.06	0.06	0.04	0.10	0.23	0.14	0.24	0.27	0.16	0.14	0.15	0.18	0.25	0.24	0.19
BaO	bdl	0.03	0.01	0.01	0.02	0.02	0.14	0.04	0.09	0.10	0.03	0.07	0.04	0.06	0.09	0.07	0.07
Na_2O	1.56	0.21	0.17	0.15	0.12	0.72	0.20	0.18	0.22	0.24	0.19	0.41	0.36	0.21	0.23	0.19	0.19
K_2O	8.28	8.88	8.20	8.00	7.99	8.29	8.88	8.59	8.80	8.76	7.90	8.58	8.23	8.59	8.63	8.57	8.69
Total	93.03	90.86	95.17	94.92	96.70	95.91	95.44	93.74	95.17	94.65	95.15	91.77	92.60	94.39	94.21	94.25	95.43
Tetrahedral																	
Si	3.47	3.38	3.40	3.30	3.29	3.38	3.26	3.30	3.26	3.26	3.32	3.28	3.33	3.29	3.28	3.28	3.29
Al	0.53	0.62	0.60	0.70	0.71	0.62	0.74	0.70	0.74	0.74	0.68	0.72	0.67	0.71	0.72	0.72	0.71
Octahedral																	
Al	1.66	1.70	1.67	1.72	1.72	1.71	1.83	1.85	1.84	1.83	1.86	1.82	1.83	1.85	1.84	1.84	1.85
Ti	-	-	0.01	0.01	-	-	0.01	0.01	0.01	0.01	-	-	-	-	0.01	0.01	-
Fe^{2+}	0.13	0.11	0.11	0.09	0.11	0.07	0.08	0.09	0.08	0.08	0.09	0.10	0.08	0.08	0.08	0.08	0.08
Mn	0.01	0.01	0.01	0.01	0.02	0.01	-	-	-	-	-	-	-	-	-	-	-
Mg	0.17	0.22	0.30	0.30	0.29	0.28	0.12	0.09	0.11	0.12	0.10	0.11	0.11	0.10	0.10	0.10	0.10
TOC[1]	1.97	2.04	2.10	2.13	2.14	2.07	2.04	2.04	2.04	2.04	2.05	2.03	2.02	2.03	2.03	2.03	2.03
OC[2]	-0.40	-0.22	-0.11	0.0	0.0	-0.15	-0.07	-0.05	-0.06	-0.07	-0.04	-0.12	-0.13	-0.09	-0.08	-0.08	-0.09
Interlayer																	
Ca	0.01	0.01	-	-	-	0.01	0.02	0.01	0.02	0.02	0.01	0.01	0.01	0.01	0.02	0.02	0.01
Na	0.20	0.03	0.02	0.02	0.02	0.09	0.03	0.02	0.03	0.03	0.02	0.05	0.05	0.03	0.03	0.02	0.02
K	0.71	0.78	0.69	0.67	0.66	0.69	0.74	0.73	0.74	0.74	0.66	0.75	0.71	0.72	0.73	0.72	0.73
LC[3]	0.93	0.83	0.71	0.69	0.68	0.80	0.81	0.77	0.81	0.81	0.70	0.82	0.78	0.77	0.80	0.78	0.78
TLC	−0.93	−0.84	−0.71	−0.70	−0.71	−0.77	−0.81	−0.75	−0.80	−0.81	−0.72	−0.84	−0.80	−0.80	−0.80	−0.80	−0.80

*All iron assumed as FeO; [1]TOC: Total octahedral cation; [2]OC: Octahedral charge; [3]LC: Layer charge; [4]TLC: Total layer charge, bdl: Below detection limit.

wt%), and kaolinite (0–11 wt%, except for 4 samples) were estimated in decreasing order (Table S2).

4.6. K-Ar dating

In order to determine the age of the magmatic rocks and to interpret geologic history, the radiometric K-Ar dating was used on the illites. Inasmuch as the rocks in this study were severely altered, an attempt was made to identify the age of the hydrothermal alteration. Thus, the examination was focused on samples that only contained illite (Figure 8). Clauer et al. (1993) studied the effect of chemical pretreatments during illite separation from rocks; they showed that radiogenic Ar is not affected during illite washing with 10% HCl. After the separation of illites from dacites, strong acids were not used. XRD was also employed to exclude impure samples. Consequently, the illite ages were 76.9 ± 2.2 – 81.7 ± 2.5 Ma in dacite-I and

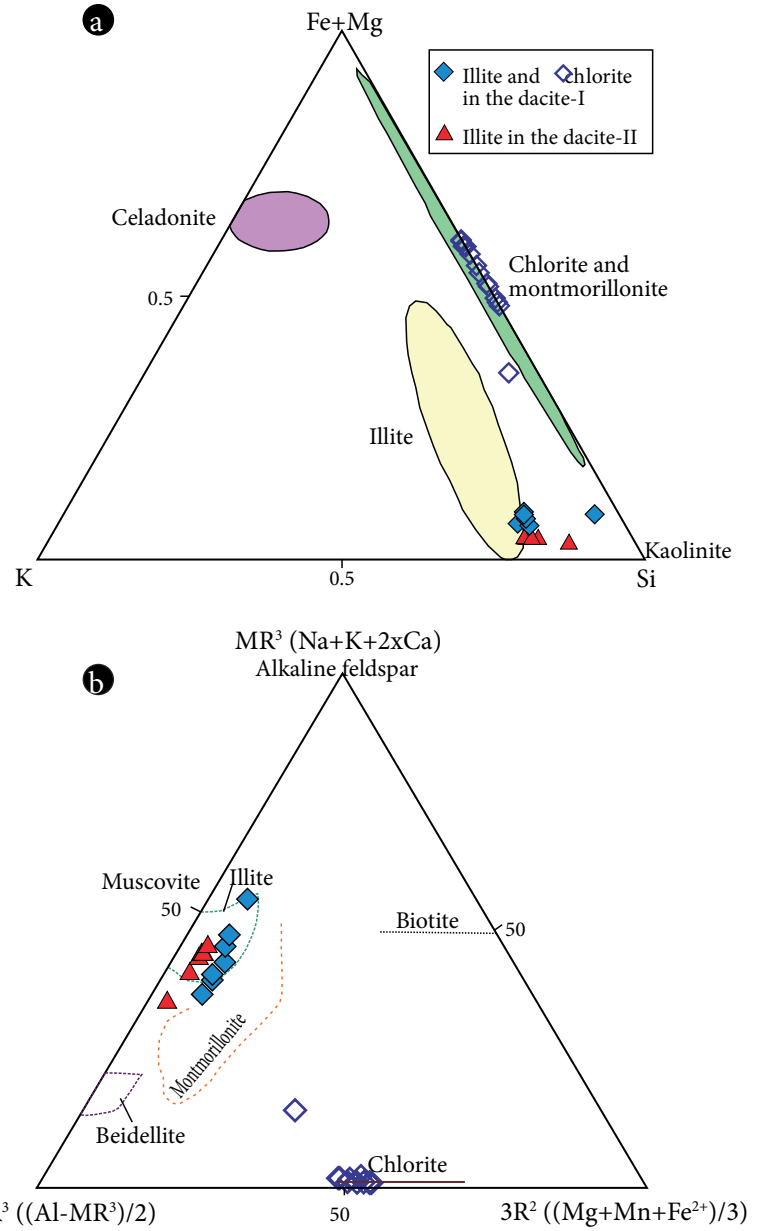

Figure 6. The chemical characteristics of illites from dacites in (Fe^{2+}+Mg)-K-Si (a) and MR^3-$2R^3$-$3R^2$ (b) ternary diagrams (after Velde, 1985; Newman and Brown, 1987).

72.6 ± 2.8 – 78.2 ± 2.3 Ma in dacite-II (Table 5). Sample 397 (78.2±2.3 Ma) from dacite-II was close to dacite-I, and thus, the K-Ar age might represent a mixed age in this sample. Overall, the illite age variations in dacite-I and dacite-II reflected different hydrothermal alteration events. Additionally, there was very little variation among the K-Ar age averages (78.7 ± 2.3 Ma for dacite-I and 75.3 ± 2.4 Ma for dacite-II), which suggests Late Cretaceous age (Campanian) for alteration (Table 5). The ages of the illites suggest that they were formed after the last volcanic episode. The age of the two illite types also indicates that dacite-I and dacite-II experienced similar hydrothermal alteration.

4.7. Stable isotope geochemistry of illites

The O and H isotopic values of the <2 μm illite clay fraction of the dacitic rocks varies within narrow limits from +8.6 to +10.2‰ and –51 to –52‰ (dacite-I), and +8.5 to +10.7‰ and –46 to –54‰ (dacite-II; Table 6). This indicates that the illites originated from very similar fluids. On the δD versus $\delta^{18}O$ diagram (Hoefs, 1973, 1987) the illites plot in

Table 3. Selected electron microprobe analyses (wt%) of chlorite in dacite-I, kaolinite in dacite-II, and structural recalculations.

Chlorite in dacite-I										Kaolinite in dacite-II
Point	#15	#16	#17	#18	#19	#20	#21	#24	#25	#131c
SiO_2	26.41	26.14	26.38	29.29	27.75	30.78	29.68	30.19	28.16	62.56
TiO_2	0.26	0.16	0.11	0.02	0.02	0.04	0.02	0.01	0.04	0.14
Al_2O_3	19.39	18.47	19.95	18.02	19.51	17.93	16.60	17.15	16.28	34.5
FeO*	20.88	20.26	21.99	12.32	19.13	13.37	12.01	13.72	12.34	1.72
MnO	0.68	0.67	0.77	0.79	1.07	0.74	0.65	0.66	0.59	bdl
Cr_2O_3	0.00	0.00	0.02	0.26	0.16	1.41	0.72	1.10	0.79	nd
NiO	0.00	0.00	0.06	0.05	0.01	0.05	0.00	0.00	0.03	nd
MgO	14.70	14.51	15.11	17.87	14.93	15.27	12.95	14.63	13.59	0.71
CaO	0.01	0.01	0.00	0.02	0.01	0.05	0.12	0.09	0.07	0.02
Na_2O	0.06	0.09	0.05	0.06	0.03	0.19	0.06	0.02	0.02	bdl
K_2O	0.05	0.03	0.04	0.06	0.04	0.07	0.04	0.03	0.02	0.15
Total	82.44	80.34	84.48	78.76	82.66	79.90	72.85	77.60	71.93	99.8
Tetrahedral										
Si	2.90	2.94	2.84	3.19	3.00	3.32	3.47	3.35	3.36	2.32
Al	1.10	1.06	1.16	0.81	1.00	0.68	0.53	0.65	0.64	1.28
Octahedral										
Al	1.41	1.39	1.37	1.50	1.49	1.60	1.76	1.60	1.65	1.51
Ti	0.02	0.01	0.01	-	-	-	-	-	-	-
Fe^{2+}	1.92	1.91	1.98	1.12	1.73	1.21	1.17	1.28	1.23	0.05
Mn	0.06	0.06	0.07	0.07	0.10	0.07	0.06	0.06	0.06	-
Cr	-	-	-	0.02	0.01	0.12	0.07	0.10	0.07	-
Ni	-	-	-	-	-	-	-	-	-	-
Mg	2.41	2.43	2.43	2.90	2.41	2.45	2.26	2.42	2.42	0.04
TOC[1]	5.82	5.80	5.86	5.61	5.74	5.45	5.32	5.46	5.43	1.60
NV[2]	0.18	0.20	0.14	0.39	0.26	0.55	0.68	0.54	0.57	
OC[3]	1.09	1.01	1.11	0.74	0.98	0.62	0.47	0.62	0.58	–1.29
Interlayer										
Ca	-	-	-	-	-	0.01	0.02	0.01	0.01	-
Na	0.01	0.02	0.01	0.01	0.01	0.04	0.01	-	0.01	-
K	0.01	-	-	0.01	0.01	0.01	0.01	-	-	0.01
LC[4]	0.02	0.02	0.01	0.02	0.02	0.07	0.06	0.02	0.03	0.01
TLC[5]	–0.01	–0.05	–0.05	–0.07	–0.02	–0.06	–0.06	–0.03	–0.06	–0.01
Fe/(Fe+Mg)	0.44	0.44	0.45	0.28	0.42	0.33	0.34	0.34	0.34	

*All iron assumed as FeO; bdl: Below detection limit; nd: Not detected; [1]TOC: Total octahedral cation; [2]NV: Numbers of vacant; [3]OC: Octahedral charge; [4]LC: Layer charge; [5]TLC: Total layer charge.

the metamorphic and primary magmatic water field (Figure 9a). Moreover, the oxygen isotopic composition shows limited variability. The dacite-I samples are found mostly in the more magmatic field than the metamorphic field. The oxygen isotopic composition of the illite in dacite-I is indicative of a magmatic rather than metamorphic signature.

Assuming that illite minerals were isotopically equilibrated with fluids at calculated temperatures

Table 4. The formation temperature values of chlorite in dacite-I.

Point	Al^{iv}	$Fe^{2+}/(Fe^{2+}+Mg)$	Ref. 1 (°C)
#15	1.10	0.44	295
#16	1.06	0.44	283
#17	1.16	0.45	315
#18	0.81	0.28	198
#19	1.00	0.42	263
#20	0.68	0.33	158
#21	0.53	0.34	110
#24	0.65	0.34	149
#25	0.64	0.34	146

Eq. (Ref. 1) used in the calculation are as follows:
T (°C) = 319 * [Al^{iv}+0.1 * [Fe/(Fe + Mg)]] – 69 (Jowett, 1991).

for chlorite associated with illite, the $\delta^{18}O$ values of equilibrated fluids may be evaluated using the oxygen isotope fractionation equation between illite and water as a function of temperature (Sheppard and Gilg, 1996). The oxygen isotope compositions of fluid or fluids equilibrated with illite were compared with the oxygen isotope composition of different solutions and rocks (Figure 9a). As expected, temperature is important for oxygen isotope composition (Figure 9b). The $\delta^{18}O$ values of the illite and fluid(s) equilibrated with the illite in the dacite-II appeared to change over a wider interval compared with those in the dacite-I at 100, 200, and 300 °C.

5. Discussion

5.1. Clay and whole-rock alteration mineralogy

The endothermic peak value of illite at ~890 °C continued the crystal structure of the illite in this study, while the

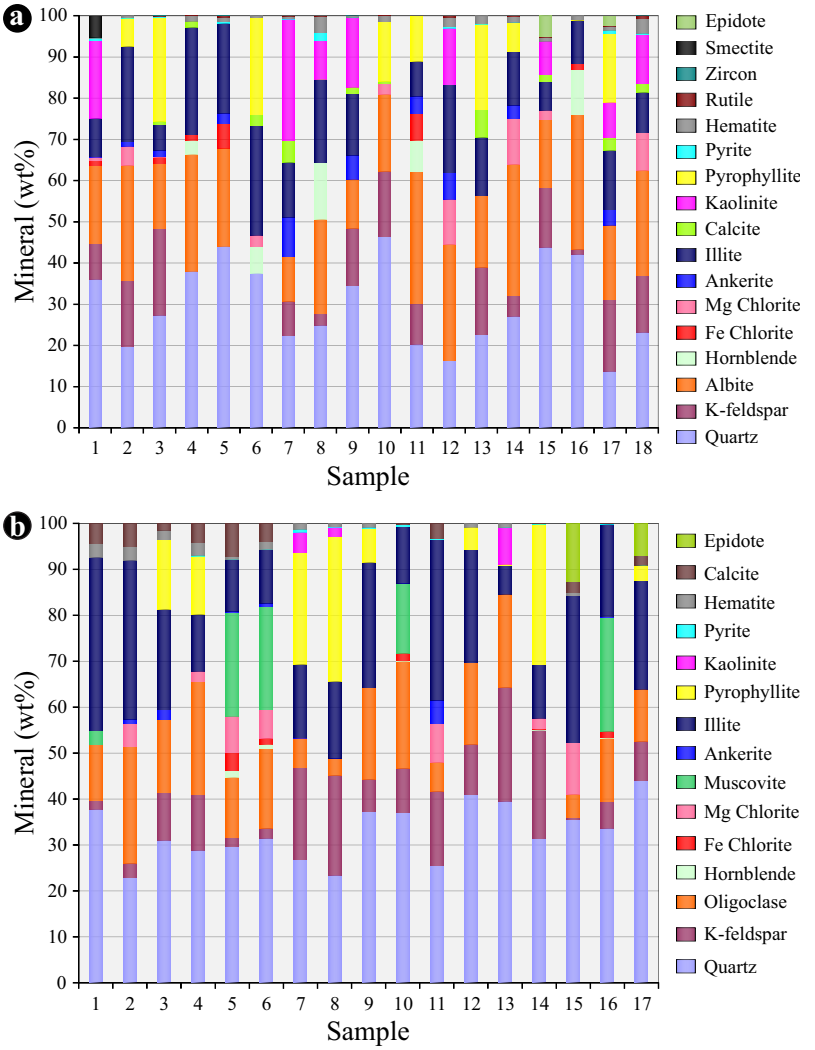

Figure 7. Mineral compositions of (a) dacite-I, and (b) dacite-II samples calculated using the MINSQ method from whole-rock major element analyses.

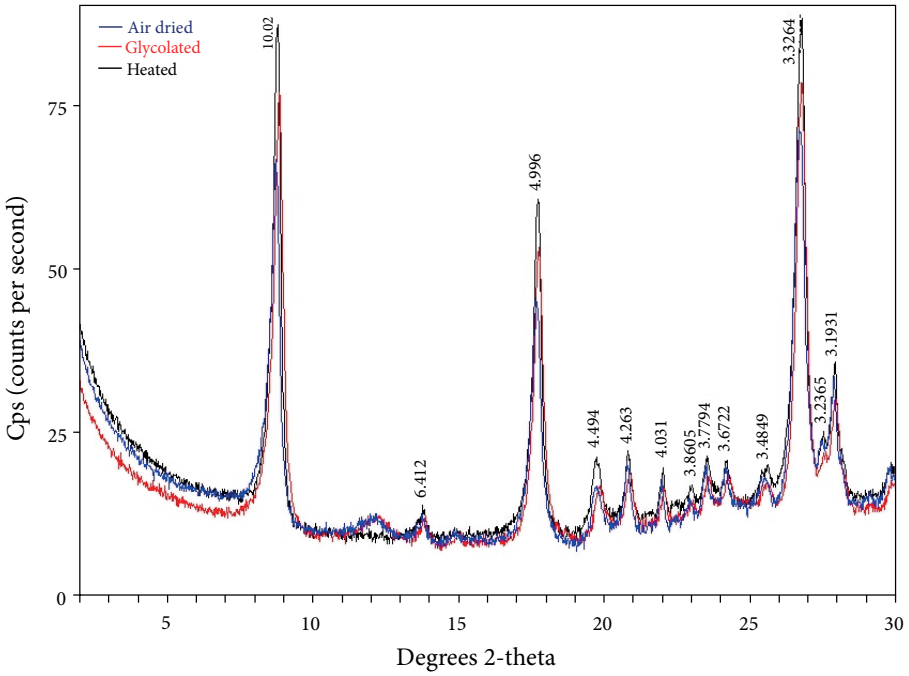

Figure 8. The oriented XRD pattern of illite in dacite-II.

Table 5. Age analyses of illites in dacites measured with K-Ar dating.

Samples	Rock type	Mineral	^{40}K (%)	Ar_{rad}, (nL/g)	$^{40}Ar_{air}$(%)	Age (Ma)
D6	Dacite-I	Illite	3.92	12.5	7.2	81.7±2.5
161			4.05	12.25	8.1	77.7±2.2
288			3.42	10.26	12	76.9±2.2
397	Dacite-II	Illite	3.32	10.11	8.7	78.2±2.3
512			4.55	12.85	4.8	72.6±2.8
496			4.61	13.51	5.2	75.3±2.1

Table 6. Isotopic analyses of illites in dacites.

Samples	Rock type	Mineral	$\delta^{18}O_{(VSMOW)}$ (‰)	$\delta D_{(SMOW)}$ (‰)	The $\delta^{18}O_{smow}$ values of fluids equilibrated with illite[a,b] (‰)						H_2O (%)
					100 °C		200 °C		300 °C		
D6	Dacite-I	Illite	10.2	–52	–2.78[a]	–3.21[b]	3.71[a]	3.27[b]	7.11[a]	6.68[b]	1.6
161			8.6	–52	–4.38[a]	–4.81[b]	2.11[a]	1.68[b]	5.52[a]	5.09[b]	3.6
288			8.6	–51	–4.38[a]	–4.81[b]	2.11[a]	1.68[b]	5.52[a]	5.09[b]	1.3
397	Dacite-II	Illite	8.5	–49	–4.48[a]	–4.91[b]	2.01[a]	1.58[b]	5.42[a]	4.99[b]	1.3
512			10.7	–54	–2.28[a]	–2.71[b]	4.21[a]	3.78[b]	7.62[a]	7.19[b]	3.2
496			10.1	–46	–2.88[a]	–3.31[b]	3.61[a]	3.18[b]	7.02[a]	6.59[b]	2.7

[a]Savin and Lee (1988); [b]Sheppard and Gilg (1996).

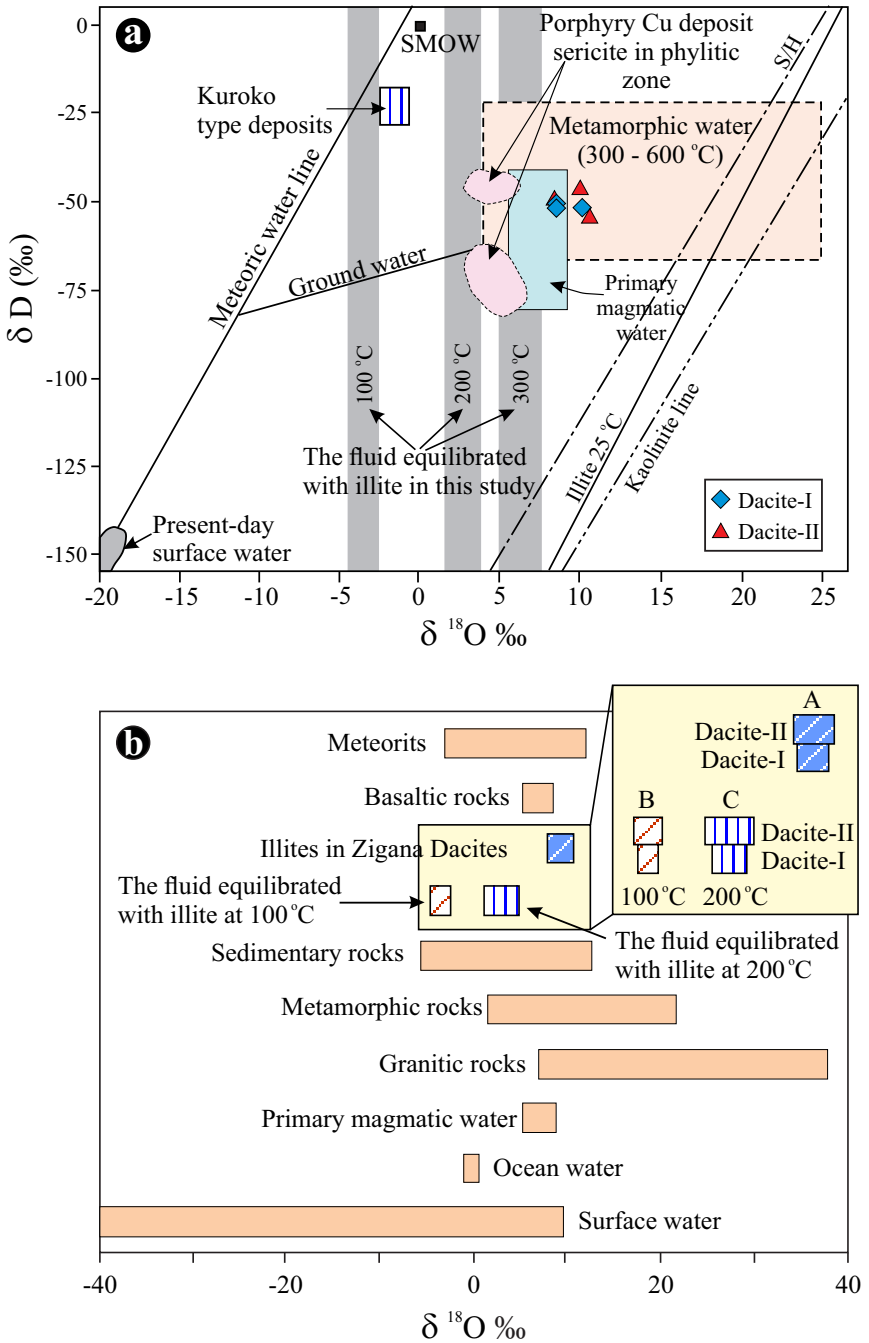

Figure 9. (a) The $\delta^{18}O$ vs.δD diagram (after Hoefs, 1987) shows the isotopic composition of Zigana Mountain illites.The equation used in the calculations is as follows: $\delta^{18}O_{illite}-\delta^{18}O_{fluid}= 1000\ \ln a(O)_{(illite\text{-}water)} =+2.39\times(10^6 xT^{-2})-3.76$ (Sheppard and Gilg, 1996). The kaolinite line and S/H (supergene/hypogene) line are from Savin and Epstein (1970) and Sheppard et al. (1969). (b) Comparison of the $\delta^{18}O$ composition of illites in different rocks (Hoefs, 1973, 1987). A: the $\delta^{18}O$ compositions of illite in dacite-I and dacite-II; B: the fluids equilibrated with illites of the dacite-I and dacite-II at 100 °C; C: the fluids equilibrated with illites of the dacite-I and dacite-II at 200 °C.

endothermic peak value of illite at ~560 °C is attributed to dehydroxylation (Figures 4a and 4b). The crystal structure of illite persisted until about 900°C, but it collapsed at higher temperatures (Van Ranst, 1998). This thermal behavior is typical of illite (Van Ranst, 1998).

The kaolinite books observed in the study (Figure 5e) suggest that they formed directly from feldspars, whereas the clearly visible tubular kaolinite forms presented themselves as alteration of feldspar surfaces (Saviona et al., 2005). The loosely textured booklets formed by the

kaolinite are typical of hydrothermal origin (Yalçın and Bozkaya, 2003). The development of authigenic kaolinite books edging feldspar in volcanics suggests a dissolution-precipitation mechanism (Kadir and Erkoyun, 2013). Thus, porous plagioclase is the result of alteration, as shown in Figure 5f.

The calculated alteration mineralogy is consistent with the results of microscopic analysis and XRD data from the dacitic rocks. Illite (6 to 50 wt%), chlorite (0 to 11 wt%), and kaolinite (0 to 11 wt%, except for 4 samples) were estimated in decreasing order with the MINSQ method, whereas illite, chlorite, kaolinite, and smectite in decreasing abundance were determined in detail by XRD studies.

5.2. Chemical properties of minerals

The negative charge in octahedral and tetrahedral sites of illite in this study is attributed to balance the interlayer charge. Illite with a layer charge >0.75 e/huc and 8% K_2O content is free of smectite layers (Weaver, 1989). Środoń et al. (1986) reported that the smectite layer decreases when the K_2O content of illite increases. The SiO_2 and Al_2O_3 contents of illites in dacites from Zigana were close to the theoretical value (51.25 wt% SiO_2 and 23.53 wt% Al_2O_3; Deer et al., 1992).The value of Mg was 0.17–0.30 (dacite-I) and 0.09–0.12 (dacite-II) atoms per formula unit. In effect, the illite had low Mg content, as presented earlier. According to Weaver and Pollard (1973), Mg-poor illites mainly formed from the decomposition of feldspar. The (Fe+Mg) contents of both rock types reflected an almost ideal muscovite composition within the field of illite (Figure 6a). Some illites in the dacitic rocks plot toward montmorillonite (Figure 6b). The Fe (0.07 to 0.13 apfu) contents of illites in dacite-I are similar to those (0.05 to 0.56 apfu) of illites in the quartz-hematite hydrothermal veins in the St. Austell Pluton, Cornwall (Psyrillos et al., 2001).

The Fe/(Fe+Mg) ratio (0.28–0.45, average 0.37; Table 3) of chlorite provides information about the origin of chlorite because its variation might reflect the relative ratios of hydrothermal solutions (Fe-rich) and seawater (Mg-rich) (Teagle and Alt, 2004). Compositions of the chlorites from the dacite-I plot in the chlorite field defined by Velde (1985) (Figure 6). The chlorites are trioctahedral, similar to those described by Maydagán et al. (2016).

The formation temperatures of chlorites, calculated according to Jowett (1991), ranged from 110 °C to 315 °C in dacite-I and reflected the physico-chemical conditions of the hydrothermal fluids. Chlorites in the propylitic zone have a relatively low (Fe+Mn) content, and form at temperatures concentrating in the range 150–300 °C (Inoue et al., 2010). The composition of chlorite in this study is similar to the chlorites in the propylitic alteration of the Altar (Argentina) Porphyry Cu-(Au) deposit formed at 214 °C to 311°C (Maydagán et al., 2016).

The Fe and Mg content of the kaolinite might have resulted in the hematite in the samples and the decomposition of volcanic glass. Therefore, it is suggested that Fe^{3+} and Mg might play an important role within the octahedral sheet, replacing Al. The low TiO_2 content (Table 3) suggests the source (hydrothermal origin) of clays (Yalçın and Bozkaya, 2003; Başıbüyük and Yalçın, 2018). Accordingly, kaolinite might have resulted from the decomposition of feldspar in the rocks.

5.3. O and H isotopic composition of illite

According to their isotopic composition, the illites plot in the metamorphic and primary magmatic water field (Figure 9a). The small variation from light to heavy oxygen in the isotopic composition of the illite might determine the effect of temperature during mineral formation (Zheng and Hoefs, 1993). Most of the dacite-I samples had a more magmatic than metamorphic signature. The dacite-II illites have different features that might reflect an origin from fluids with different isotopic properties.

The $\delta^{18}O$ values of the isotopically equilibrated fluid for chlorite and illite were evaluated as a function of temperature (Figure 9). According to this, the δO value of the fluid or fluids increases when the temperature increases. So, the effect of temperature is important to increase the oxygen isotopic composition of illite.

5.4. The formation process for clay minerals and properties of fluids causing clay alteration

The altered dacitic rocks consist of illite, Fe-Mg chlorite, kaolinite, and smectite. This paragenesis indicates that the rocks were exposed to hydrothermal alteration. The occurrence of smectite is indicative of alteration at neutral to alkaline pH in felsic rocks (Inoue, 1995), and these minerals may be considered as intermediate products in the smectite to illite transformation with increasing temperature. Illite prevailed and might overprint preexisting smectite in the study area. Moreover, pH is one of the main factors controlling the mineral formation and paragenesis (Barnes, 1979). Kaolinite formed in an acidic environment where the pH was around 3 to 4 (Sillitoe, 1993; Arribas, 1995). The pH data (3.64 to 4.25; Sipahi, 2005) in this study supports this. Illite formed under weak alkaline conditions, at pH 7–8. Typically, illites form through hydrothermal alteration or weathering at pH 7–8 in K- and Al-rich rocks, while chlorite forms at higher pH values of 7.5–9.5 (Barnes, 1979; Large et al., 2001). Weaver and Pollard (1973) showed that most kaolinites resulted from the leaching of alkaline rocks by acidic solutions. In this study, the scarcity of kaolinite

suggests the existence of local fluctuations of pH in the rock, reflecting differential leaching. The environment was neutral with increasing pH after kaolinite was formed, and then weak alkaline environment conditions began to form. In this environment, it resulted in the formation of illite from an alteration of K-feldspar without K-supply and the formation of chlorite from Fe-Mg minerals such as biotite without significant fluctuations in pH.

The calculated geothermometer value ranges from 100–300 °C; accordingly, chlorite formed over a large temperature interval. In general, kaolinite forms under low-temperature conditions (<150–200 °C). The illite in $2M_1$ polytypes (Sipahi, 2005) presented a stable form of muscovite in the hydrothermal experiments. Inasmuch as the stability temperature of illite ranges at about 125–300°C, it can be used as a geothermometer for prograde thermal effects covering the epithermal (100–200°C) and mesothermal (200–300°C) intervals (Guilbert and Park, 1985). Additionally, illite formed in the presence of weakly CO_2-rich fluids (Horton, 1985; Simmons and Browne, 1990).

Chlorite was observed as a replacement of mafic phenocrysts (amphibole and biotite). In the study area, chlorite alteration generally occupies the inner alteration zone (propylitic) and passes outward into illite alteration (sericitic) zone. These chlorites havea low Fe/(Fe + Mg) ratio, with an average of 0.37 in this study. Shikazono and Kawahata (1987) noted that Fe/Mg ratios of chlorite in altered rocks are assumed to be in equilibrium with a fluid phase and pyrite. The exchange of Fe^{2+}, Mg, and Mn^{2+} between chlorite and the hydrothermal fluid is related to pH, oxygen fugacity, temperature, and total dissolved sulfur (Murakami, 2008). Moreover, the Fe/(Fe+Mg) ratio of hydrothermal chlorite might decrease because the iron content of chlorite decreases with an increase in oxygen fugacity in the region where H_2S is dominant (Shikazono and Kawahata, 1987). Mg-rich chlorite can result from the interaction of cold seawater with hot hydrothermal fluids (Teagle and Alt, 2004).

Based on these reactions, this study can now easily deduce why illites are rarely seen together with chlorite in the area (e.g., Large, 1992; Lentz, 1999; Schardt et al., 2001). In the study area, calcite was determined in the illite-chlorite-silica (propylitic) zone within a fracture in dacite. The source of Ca might be plagioclase and hornblende. The formation of calcite can be explained as follows, equations (1) and (2):

$$CaAl_2Si_2O_6 + 2Na^+ + 4SiO_2 + 2H_2O \rightarrow 2NaAlSi_3O_8 \ (albite) + Ca^{2+} + 4H^+ \quad (1)$$

$$CaO + CO_2 + H^+ + OH^- \rightarrow CaCO_3 \ (calcite) + H_2O \quad (2)$$

H- and O-isotope studies suggest that the fluids from which the illite formed mainly correspond to magmatic fluids, whereas other fluids (seawater, underground water, etc.) only play a minor role in illite formation. Thus, the formation of clay minerals in dacites reflects these main alteration conditions: (1) the hydrothermal fluids changed from slightly acidic (practically neutral) to moderately alkaline; (2) the temperature is below 300°C for clay minerals; and (3) the isotope values of illite mainly indicate a magmatic origin.

6. Conclusions

The results of this study are summarized below:

1. Illite and chlorite dominate in the study area, while smectite and kaolinite are rarely found. All these hydrothermal mineral assemblages are accompanied by secondary quartz. Clay mineralogy studies indicate that the illite-chlorite-silicification (propylitic) zone and illite-silicification (sericitic) zone accompanying the kaolinite are present in the dacitic rocks.

2. The illites are Fe- and Mg-poor and reflect an epithermal and mesothermal character. Chlorites have a low Fe/(Fe+Mg) ratio, which might have resulted from the enrichment of low temperature (100–300 °C) and oxidized water in the hydrothermal alteration systems. Illite occurs under weaker alkaline conditions compared with chlorite.

3. Isotopic data show that magmatic fluids dominate illite formation. The hydrothermal overprinting mainly occurred at 78.7±2.3 Ma in dacite-I and 75.3±2.4 Ma in dacite-II (i.e. Campanian), based on the K-Ar dating of the illite.

4. Clay minerals in the dacitic rocks developed with different hydrothermal alteration degrees in rocks under acidic-weak alkaline conditions at the meso-epithermal phase.

Acknowledgments

This research is a part of the PhD study of the first author. The authors thank Dr. Muazzez Çelik Karakaya from Konya Technical University (Turkey) for informations and comments about clay minerals, Dr. Tayfur Küçükömeroğlu from Karadeniz Technical University (Trabzon, Turkey) for XRD measurements, Karadeniz Technical University Research Funds (Project No: 2001.112.005.1) for financial support and Dr. Yakov Kapusta for the K-Ar dating. The authors thank Dr. George Christidis for helpful comments and Dr. Maarten A.T.M. Broekmans for the improved the content of the manuscript.

References

Abdioğlu E, Arslan M (2008). Alteration mineralogy and geochemistry of the hydrothermally altered rocks of the Kutlular (Sürmene) massive sulfide deposit, NE Turkey. Turkish Journal of Earth Sciences 18: 139-162.

Abdioğlu E, Arslan M, Kadir S, Temizel İ (2015). Alteration mineralogy, lithochemistry and stable isotope geochemistry of the Murgul (Artvin, NE Turkey) volcanic hosted massive sulfide deposit: Implications for the alteration age and ore forming fluids. Ore Geology Reviews 66: 219-242.

Akaryalı E (2016). Geochemical, fluid inclusion and isotopic (O, H and S) constraints on the origin of Pb-Zn±Au vein-type mineralizations in the Eastern Pontides Orogenic Belt (NE Turkey). Ore Geology Reviews 74: 1-14.

Akaryalı E, Akbulut K (2016). Constraints of C-O-S isotope compositions and the origin of the Ünlüpınar volcanic-hosted epithermal Pb-Zn±Au deposit, Gümüşhane, NE Turkey. Journal of Asian Earth Sciences 117: 119-134.

Akaryalı E, Tüysüz N (2013). The genesis of the slab window-related Arzular low-sulfidation epithermal gold mineralization (eastern Pontides, NE Turkey). Geoscience Frontiers 4 (4): 409-421.

Akyürek S, Sipahi F (2014). Mineralogy and hydrotermal alteration of Kıbletepe (Trabzon, NE Turkey) volcanogenic massive Zn-Cu mineralization. Gümüşhane University Journal of Science and Technology Institute 4 (1): 77-96 (in Turkish with English abstract).

Altun Y (1972). Geology of the Madenköy (1) area. Mineral Research and Exploration General Directorate of Turkey (MTA) Report, 553. Ankara, Turkey: MTA, pp. 1-10.

Arribas AJR (1995). Characteristics of high-sulfidation epithermal deposits, and their relation to magmatic fluid. In: Thompson JFH (editor). Magmas, Fluids, and Ore Deposits. Mineralogical Association of Canada, Short Course 23. Quebec, Canada: Mineralogical Association of Canada, pp. 419-454.

Arslan M, Tüysüz N, Korkmaz S, Kurt H (1997). Geochemistry and petrogenesis of the eastern Pontide volcanic rocks, northeast Turkey. Chemie der Erde-Geochemistry 57: 157-187.

Barnes HL (1979). Geochemistry of Hydrothermal Ore Deposits. New York, NY, USA: John Wiley and Sons Inc.

Barret TJ, Cattalani S, MacLean WH (1993). Volcanic lithogeochemistry and alteration at the Delbridge massive sulphide deposits, Noranda Quebec. Journal of Geochemical Exploration 48: 135-173.

Barrett TJ, MacLean WH (1991). Chemical, mass, and oxygen isotope changes during extreme hydrothermal alteration of an Archean rhyolite, Noranda, Qebec. Economic Geology 86 (2): 406-414.

Başıbüyük Z, Yalçın H (2018). Mineralogy, petrography and origin of hydrothermal alteration in Eocene magmatites in Central Anatolia (Sivas-Turkey). Bulletin of the Mineral Research and Exploration 158: 143-166.

Bektaş O, Şen C, Atıcı Y, Köprübaşı N (1999). Migration of the Upper Cretaceous subduction-related volcanism toward the back-arc basin of the eastern Pontide magmatic arc (NE Turkey). Geological Journal 34: 95-106.

Boztuğ D, Jonckheere R, Wagner GA, Yeğingil Z (2004). Slow Senonian and fast Palaeocene-Early Eocene uplift of the granitoids in the Central Eastern Pontides, Turkey: apatite fission-track results. Tectonophysics 382: 213-228.

Buser S, Cvetic S (1973). Geology of the environs from the Murgul copper deposits, Turkey. Bulletin of the Mineral Research and Exploration 81: 22-45 (in Turkish).

Çağatay MN (1993). Hydrothermal alteration associated with volcanogenic massive sulphide deposits: examples from Turkey. Economic Geology 88: 606-621.

Callaghan T (2001). Geology and host-rock alteration of the Henty and Mount Julia gold deposits, Western Tasmania. Economic Geology 96: 1073-1088.

Cathelineau M (1988). Cation site occupancy in chlorites and illites as a function of temperature. Clay Minerals 23: 471-485.

Cathelineau M, Nieva D (1985). A chlorite solid solution geothermometer: The Los Azufres (Mexico) geothermal system. Contributions to Mineralogy and Petrology 91: 235-244.

Çelik M, Karakaya N, Temel A (1999). Clay minerals in hydrothermal altered volcanic rocks, eastern Pontides, Turkey. Clays and Clay Minerals 77 (6): 708-717.

Çiftçi E, Hagni RD (2005). Mineralogy of the Lahanos deposit a Kuroko-type volcanogenic massive sulfide deposit from the eastern Pontides (Giresun, NE Turkey). Geological Bulletin of Turkey 48 (1): 55-64.

Çiftçi E, Kolaylı H, Tokel S (2005). Lead-arsenic soil geochemical study as an exploration guide over the Killik volcanogenic massive sulfide deposit, Northeastern Turkey. Journal of Geochemical Exploration 86 (1): 49-59.

Clauer N, Chaudhuri S, Kralik M, Bonnot-Courtois C (1993). Effect of experimental leaching on Rb-Sr and K-Ar isotopic system and REE contents of diagenetic illite. Chemical Geology 103: 1-6.

Clayton RN, Mayeda TK (1963). The use of bromine penta-fluoride in the extraction of oxygen from oxides and silicates for isotopic analysis. Geochimica et Cosmochimica Acta 27: 43-52.

Dana JD (1993). Manuel of Mineralogy. 21st ed. Hoboken, NJ, USA: John Wiley and Sons, Inc. , p. 681.

Deer WA, Howie RA, Zussman J (1992). An introduction to the rock forming minerals, 2nd ed.. London, UK: Longman, p. 696.

Dokuz A (2011). A slab detachment and delamination model for the generation of Carboniferous high-potassium I-type magmatism in the eastern Pontides, NE Turkey: The Köse composite pluton. Gondwana Research 19: 926-944.

Elliot-Meadows S, Appleyard EC (1991). The alteration geochemistry and petrology of the Lar Lake Cu-Zn deposit, Lynn lake area, Manitoba, Canada. Economic Geology 86: 486-505.

Eyüboğlu Y, Santosh M, Yi K, Tüysüz N, Korkmaz S et al. (2014). The eastern Black Sea-type volcanogenic massive sulfide deposits: geochemistry, zircon U-Pb geochronology and an overview of the geodynamics of ore genesis. Ore Geology Reviews 59: 29-54.

Gedik A, Ercan T, Korkmaz S, Karataş S (1992). Rize-Fındıklı-Çamlıhemşin arasında (Doğu Karadeniz) yer alan mağmatik kayaçların petrolojisi ve Doğu Ponditlerdeki bölgesel yayılımları. Geological Bulletin of Turkey 35: 15-38 (in Turkish).

Guilbert JM, Park CF Jr (1985). The geology of ore deposits. New York, NY, USA: W.H. Freeman and Company, p. 985.

Gümüş A (1998). İç olaylara bağlı maden yatakları. İzmir, Turkey: Bilim Ofset (in Turkish).

Gündoğdu MN, Yılmaz O (1984). Kil mineralojisi yöntemleri. In: I. Ulusal Kil Konferansı; Adana, Turkey. pp. 319-330 (in Turkish).

Güven İH (1993). Doğu Karadeniz Bölgesi'nin 1/25.000 ölçekli jeolojisi ve komplikasyonu. Ankara, Turkey: Mineral Research and Exploration General Directorate of Turkey (MTA) (in Turkish).

Hermann W, Berry RF (2002). MINSQ-a least squares spreadsheet method for calculating mineral proportions from whole rock major element analyses. Geochemistry: Exploration, Environment, Analysis 2: 361-368.

Hill IG, Worden RH, Meighan IG (2000). Yttrium: the immobility-mobility transition during basaltic weathering. Geology 28: 923-926.

Hoefs J (1973). Stable isotope geochemistry. New York, NY, USA: Springer-Verlang.

Hoefs J (1987). Stable isotope geochemistry. Berlin, Germany: Springer-Verlang Berlin Heidelberg.

Horton DG (1985). Mixed-layer illite/smectite as a paleotemperature indicator in the Amethyst vein system, Creede district, Colorado, USA. Contributions to Mineralogy and Petrology 91: 171-179.

Inoue A (1995). Formation of clay minerals in hydrothermal environments. In: Velde B (editor). Origin and mineralogy of clays. Berlin, Germany: Springer, pp. 268-329.

Inoue A, Kurokawa K, Hatta T (2010). Application of chlorite geothermometry to hydrothermal alteration in Toyoha geothermal system, southwestern Hokkaido, Japan. Resource Geology 60: 52-70.

Jackson ML (1956). Soil chemical analysis-advanced course: Published by the author. 1st ed. Department of Soil Science, University of Wisconsin, Madison, Wisconsin, p. 991.

JICA (1986). The republic of Turkey report on the cooperative mineral exploration of Gümüşhane area, consolidated report. Ankara, Turkey: Japanese International Cooperation Agency, p. 146 (in Turkish).

Jowett EC (1991). Fitting iron and magnesium into the hydrothermal chlorite geothermometer. In: GAC/MAC/SEG Joint Annual Meeting, Program with Abstracts 16, A62; Toronto, Canada.

Kadir S, Erkoyun H (2013). Genesis of the hydrothermal Karaçayır kaolinite deposit in Miocene volcanics and Palaeozoic metamorphic rocks of the Uşak-Güre Basin, western Turkey. Turkish Journal of Earth Sciences 22: 444-468.

Karakaya N, Karakaya MÇ (2001a). Mineralogic and geochemical properties of hydrothermal alteration types of Şaplıca (Şebinkarahisar, Giresun) volcanites. Geological Bulletin of Turkey 44 (2): 75-90 (in Turkish).

Karakaya N, Karakaya MÇ (2001b). Hydrothermal alteration of the Şaplıcavolcanic rocks, Şebinkarahisar, Turkey. International Geology Review 43: 953-962.

Karakaya N, Karakaya MÇ, Nalbantçılar MT, Yavuz F (2007). Relation between spring-water chemistry and hydrothermal alteration in the Şaplıca volcanic rocks, Şebinkarahisar (Giresun, Turkey). Journal of Geochemical Exploration 93: 35-46.

Karakaya MÇ, Karakaya N, Küpeli Ş (2011a). Mineralogical and geochemical properties of the Na- and Ca-bentonites of Ordu (Ne Turkey). Clays and Clay Minerals 59 (1): 75-94.

Karakaya MÇ, Karakaya N, Bakır S (2011b). Some properties and potential applications of the Na- and Ca-bentonites of Ordu (N.E. Turkey). Applied Clay Science 54: 159-165.

Karakaya MÇ, Karakaya N, Küpeli Ş, Yavuz F (2012). Mineralogy and geochemical behavior of trace elements of hydrothermal alteration types in the volcanogenic massive sulfide deposits, NE Turkey. Ore Geology Reviews 48: 197-224.

Karakaya MÇ, Karakaya N, Küpeli Ş, Karadağ MM, Kırmacı M (2015). Potential bioaccumulator mosses around massive sulfide deposits in the vicinity of the Giresun area, Northeast Turkey. Clean – Soil, Air, Water 43 (1): 27-37.

Karslı O, Dokuz A, Uysal İ, Aydın F, Chen B et al. (2010). Relative contributions of crust and mantle to generation of Campanian high-K calc-alkaline I-type granitoids in a subduction setting, with special reference to the Harşit Pluton, Eastern Turkey. Contributions to Mineralogy and Petrology 160: 467-487.

Kaygusuz A, Arslan M, İlbeyli N, Sipahi F (2012b). Doğu Pontid kuzey zonu ve kuzey-güney zon geçişinde yüzeylenen Kretase-Paleosen yaşlı granitoyidik sokulumların petrokimyası, Sr-Nd-Pb-O izotop jeokimyası, jeokronolojisi ve jeodinamik gelişimi, Tübitak Çaydag Project No: 109Y052 final report. Ankara, Turkey: TÜBİTAK, p.175 (in Turkish with English abstract).

Kaygusuz A, Arslan M, Siebel W, Sipahi F, İlbeyli N (2012). Geochronological evidence and tectonic significance of Carboniferous magmatism in the southwest Trabzon area, eastern Pontides, Turkey. International Geology Review 54 (15): 1776-1800.

Kaygusuz A, Arslan M, Siebel W, Sipahi F, İlbeyli N et al. (2014). LA-ICP MS zircon dating, whole-rock and Sr-Nd-Pb-O isotope geochemistry of the Camiboğazı pluton, Eastern Pontides, NE Turkey: Implications for lithospheric mantle and lower crustal sources in arc-related I-type magmatism. Lithos 192-195: 271-290.

Kaygusuz A, Arslan M, Sipahi F, Temizel İ (2016). U-Pb zircon chronology and petrogenesis of carboniferous plutons in the northern part of the Eastern Pontides, NE Turkey: Constraints for Paleozoic magmatism and geodynamic evolution: Gondwana Research 39: 327-346.

Kaygusuz A, Aydınçakır E (2011). Petrogenesis of a late cretaceous composite pluton from the eastern Pontides: The Dağbaşı pluton, NE Turkey. Neues Jahrbuch für Mineralogie-Abhandlungen 188: 211-233.

Kaygusuz A, Chen B, Aslan Z, Siebel W, Şen C (2009). U-Pb zircon SHRIMP ages, geochemical and Sr-Nd isotopic compositions of the early Cretaceous I-type Sarıosman pluton, Eastern Pontides, NE Turkey. Turkish Journal of Earth Sciences 18: 549-581.

Kaygusuz A, Şen C (2011). Calc-alkaline I-type plutons in the eastern Pontides, NE Turkey: U-Pb zircon ages, geochemical and Sr-Nd isotopic compositions. Chemie der Erde-Geochemistry 71: 59-75.

Kaygusuz A, Siebel W, İlbeyli N, Arslan M, Satır M et al. (2010). Insight into magma genesis at convergent plate margins-a case study from the eastern Pontides (NE Turkey). Neues Jahrbuch für Mineralogie-Abhandlungen 187 (3): 265-287.

Kaygusuz A, Sipahi F, İlbeyli N, Arslan M, Chen B et al. (2013). Petrogenesis of the Late Cretaceous Turnagöl intrusion in the eastern Pontides: Implications for magma genesis in the arc setting. Geoscience Frontiers 4: 423-438.

Kazmin VG, Sbortshikov IM, Ricou LE, Zonenshain LP, Boulin J et al. (1986). Volcanic belts as markers of the Mesezoic-Cenozoic evolution of Tethys. Tectonophysics 123: 123-152.

Keller WD (1976). Scanning electron micrographs of kaolins collected from diverse environments of origins I. Clays and Clay Minerals 24: 107-113.

Kunze GW (1965). Pretreatments for mineralogical analysis. In: Black CA (editor). Methods of soil analysis part I. Physical and mineralogical properties including statistics of measurement and sampling. Madison, Wisconsin, USA: Agronomy Society of America Inc., pp. 568-577.

Large RR (1992). Australian volcanic-hosted massive sulphide deposits: features, styles, and genetic models. Economic Geology 87: 549-572.

Large RR, Allen RL, Blake MD, Hermann W (2001). Hydrothermal alteration and volatile element halos for the Rosebery K lens volcanic-hosted massive sulfide deposit, western Tasmania. Economic Geology 96: 1055-1072.

Lentz DR (1999). Petrology, geochemistry, and oxygen isotope interpretation of felsic volcanic rocks and related rocks hosting the Brunswick No. 6 and No. 12 massive sulfide deposits, Bathurst Mining Camp, New Brunswick, Canada. Economic Geology 94: 57-86.

MacLean WH (1990). Mass change calculations in altered rock series. Mineralium Deposita 25: 44-49.

MacLean WH, Barrett TJ (1993). Lithochemical techniques using immobile elements. Journal of Geochemical Exploration 48: 109-133.

MacLean WH, Kranidiotis P (1987). Immobile elements as monitors of mass transfer in hydrothermal alteration: Phelps Dodge massive sulfide deposit, Matagami, Quebec. Economic Geology 82: 951-962.

Maydagán L, Franchini M, Impiccini A, Lentz D (2016). Phyllosilicates geochemistry and distribution in the Altar porphyry Cu-(Au) deposit, Andes Cordillera of San Juan, Argentina: applications in exploration, geothermometry, and geometallurgy. Journal of Geochemical Exploration 167: 83-109.

Mehra OP, Jackson ML (1960). Iron oxides removed from soils and clays by a dithionite–citrate system buffered with sodium bicarbonate. Clays and Clay Minerals 7: 317-327.

Moore WJ, McKee EH, Akıncı Ö (1980). Chemistry and chronology of plutonic rocks in the Pontid mountains, northern Turkey. In: Jankovic S, Sillitoe RH (editors). European Copper Deposits. Belgrade, Serbia: UNESCO-IGCP, pp. 209-216.

MTA-General Directorate of Mineral Research and Exploration (2011). Geological map of Turkey: MTA general directorate of mineral research and exploration: Ankara, Turkey.

Murakami H (2008). Variations in chemical composition of clay minerals and magnetic susceptibility of hydrothermally altered rocks in the Hishikari epithermal gold deposit, SW Kyushu, Japan. Resource Geology 58: 1-24.

Nebioğlu TY (1975). Geologic map of the Madenköy (1) area, 1/1000 scaled quadrangle (in Turkish). Ankara, Turkey: MTA (Mineral Research and Exploration General Directorate of Turkey).

Newman A, Brown G (1987). The chemical constitution of clays. In: Newman A (editor). Chemistry of Clays and Clay Minerals. Mineralogical Society, London, Monograph 6. Harlow, Essex, UK: Longmans, p. 129.

Okay AI, Şahintürk Ö (1997). Geology of the eastern Pontides. in Regional and Petroleum Geology of the Black Sea and Suraunding Regions. In: Robinson A (editor). Memoir 68. Tulsa, OK, USA: AAPG, pp. 291-311.

Özgür N (1993). Volcanogenic massive sulfide deposits in the east Pontic metallotect. Resource Geology 17: 180-185.

Pearce JA (1996). A user's guide to basalt discrimination diagrams. In: Wyman DA (editor). Trace element geochemistry of volcanic rocks: Applications for massive sulphide exploration. Geological Association of Canada, Short Course Notes 12. St. John's, NL, Canada: Geological Association of Canada, pp. 79-113.

Pejatoviç S (1979). Metallogeny of the Pontid-type massive sulfide deposits. Special Publication No: 177. Ankara, Turkey: MTA (Mineral Research & Exploration General Directorate of Turkey).

Psyrillos A, Manning DAC, Burley SD (2001). The nature and significance of illite associated with quartz-hematite hydrothermal veins in the St. Austell pluton, Cornwall, England. Clay Minerals 36: 585-597.

Savin SM, Epstein S (1970). The oxygen isotopic compositions of coarse grained sedimentary rocks and minerals. Geochimica et Cosmochimica Acta 34: 323-329.

Savin SM, Lee M (1988). Isotopic studies of phyllosilicates. In: Bailey SW (editor). Hydrous Phyllosilicates. Reviews in Mineralogy, 19. Washington, DC, USA: Mineralogical Society of America, pp. 189-223.

Saviona G, Violo M, Pieruccini U, Lopes da Silva ET (2005). Kaolin deposits from the northern sector of the Cunene anorthosite complex (Southern Angola). Clays and Clay Minerals 53 (6): 674-685.

Schardt C, Cooke DR, Gemmell JB, Large RR (2001). Geochemical modeling of the zoned footwall alteration pipe, Hellyer volcanic-hosted massive sulfide deposits, western Tasmania, Australia. Economic Geology 96: 1037-1054.

Schmid R (1981). Descriptive nomenclature and classification of pyroclastic deposits and fragments: Recommendations of the IUGS Subcommission on the Systematics of Igneous Rocks. Geology 9: 41-43.

Schnieder H-J, Özgür N, Palacios CM (1988). Relationship between alteration, rare earth element distribution, and mineralization of the Murgul copper deposit, northeastern Turkey. Economic Geology 83: 1236-1246.

Schroeder PA (2018). Clays in the critical zone. Cambridge, UK: Cambridge University Press.

Şengör AMC, Yılmaz Y (1981). Tethyan evolution of Turkey: a plate tectonic approach. Tectonophysics 75: 181-241.

Sheppard SMF, Gilg HA (1996). Stable isotope geochemistry of clay minerals. Clay Minerals 31: 1-24.

Sheppard SMF, Nielsen RL, Taylor HP (1969). Oxygen and hydrogen isotope ratios of clay minerals from porphyry copper deposits. Economic Geology 64: 755-777.

Shikazono N, Kawahata H (1987). Compositional differences in chlorite from hydrothermally altered rocks and hydrothermal ore deposits. Canadian Mineralogist 25: 465-474.

Sillitoe RH (1993). Epithermal models: genetic types, geometrical controls and shallow features. In: Kirkham RV, Sinclair WD, Thorpe RI, Duke JM (editors). Mineral Deposit Modeling. Geological Association of Canada, Special Paper 40. St. John's, NL, Canada: Geological Association of Canada, pp. 403-417.

Simmons SF, Browne PRL (1990). Mineralogic, alteration and fluid inclusion studies of epithermal gold-bearing veins at the Mt. Muro prospect, Central Kalimantan (Borneo). Indonesia. Journal of Geochemical Exploration 35: 63-104.

Sipahi F (2005). Mineralogy and geochemistry of hydrothermal alterations in Zigana mountain (Torul-Gümüşhane) volcanics. PhD Dissertation, Karadeniz Technical Universty, Trabzon, Turkey (in Turkish with English abstract).

Sipahi F (2011). Formation of skarns at Gümüşhane (Northeastern Turkey). Neues Jahrbuch für Mineralogie-Abhandlungen 188 (2): 169-190.

Sipahi F (2017). Geochemistry and petrogenesis of Kalınçam (Tonya-Trabzon, NE Turkey) area Late Cretaceous aged volcanic rock. Gümüşhane University Journal of Science and Technology Institute 7 (2): 102-127 (in Turkish with English abstract).

Sipahi F, Akpınar İ, Saydam Eker Ç, Kaygusuz A, Vural A et al. (2017). Formation of the Eğrikar (Gümüşhane) Fe-Cu skarn type mineralization in NE Turkey: U-Pb zircon age, lithogeochemistry, mineral chemistry, fluid inclusion, and O-H-C-S isotopic compositions. Journal of Geochemical Exploration 182 (Part A): 32-52.

Sipahi F, Gücer MA, Sadıklar MB (2019). Zigana Dağı (Gümüşhane, KD Türkiye) Dayklarının Jeokimyası ve Jeolojik Anlamı. Yerbilimleri 40 (3): 293-325 (in Turkish with English abstract).

Sipahi F, Gücer MA, Saydam Eker Ç (2020). Geochemical composition of magnetite from different iron skarn mineralizations in NE Turkey: implication for source of ore forming fluids. Arabian Journal of Geosciences 13 (2): (1-15).

Sipahi F, Sadıklar MB (2010).The mineralogy and mass change of the Zigana (Gümüşhane) volcanics of NE Turkey. Geological Bulletin of Turkey 53 (2-3): 97-128.

Sipahi F, Sadıklar MB (2014). Geochemistry of dacitic volcanics in the Eastern Pontides (NE Turkey). Geochemistry International 52 (4): 296-315.

Sipahi F, Sadıklar MB, Şen C (2014). The geochemical and Sr-Nd isotopic characteristicsof Murgul (Artvin)volcanics in the Eastern Black Sea Region (NE Turkey). Chemie der Erde-Geochemistry 74 (3): 331-342.

Środoń J, Morgan DJ, Eslinger EV, Eberl DD, Karlinger MR (1986). Chemistry of illite/smectite and end-member illite. Clays and Clay Minerals 34 (4): 368-378.

Taner MF (1977). Etudagéologique et pétrographique de la région de Güneyce-İkizdere, située au sud de Rize (Pontides orientales, Turquie). PhD Dissertation, Universite de Geneve, Geneve, Switzerland.

Teagle DAH, Alt J (2004). Hydrothermal alteration of basalts beneath the bent hill massive sulfide deposit, Middle Valley, Juan de Fuca Ridge. Economic Geology 99: 561-584.

Topuz G, Altherr R, Schwarz WH, Dokuz A, Meyer H-P (2007). Variscan amphibolite-facies rocks from the Kurtoğlu metamorphic complex (Gümüşhane area, Eastern Pontides, Turkey). International Journal of Earth Sciences 96 (5): 861-873.

Topuz G, Altherr R, Siebel W, Schwarz WH, Zack T et al. (2010). Carboniferous high-potassium I-type granitoid magmatism in the Eastern Pontides: the Gümüşhane pluton (NE Turkey). Lithos 116 (1): 92-110.

Tüysüz N (2000). Geology, lithogeochemistry and genesis of the Murgul massive sulfide deposit, NE-Turkey. Chemie der Erde-Geochemistry 60: 231-250.

Van Ranst E (1998). Analysis and dynamics of clays. Physical Land Resources, International Interuniversitary Post-Graduate Programmes, Textbook, Universiteit Gent, Belgium.

Velde B (1985). Clay minerals: A physic-chemical explanation of their occurrence. Developments in Sedimentology. Amsterdam, Netherlands: Elsevier, p. 427.

Weaver CE (1989). Clay, muds and shales. Developments in Sedimentology, 44. Amsterdam, Netherlands: Elsevier, p. 819.

Weaver CE, Pollard LD (1973). The chemistry of clay minerals. Developments in Sedimentology, 15. Amsterdam, Netherlands: Elsevier, p. 213.

Winchester JA, Floyd PA (1977). Geochemical discrimination of different magma series and their differentiation products using immobile elements. Chemical Geology 20: 325-343.

Yalçın H, Bozkaya, Ö (2003). Mineralogy and geochemistry of hydrotermal kaolinite and IS occurences, (Yıldızeli-Akdağmadeni) W-Sivas. Geological Bulletin of Turkey 46: 1-23.

Yılmaz-Şahin S (2005). Transition from arc- to post-collision extensional setting revealed by K-Ar dating and petrology: An example from the granitoids of the eastern Pontide igneous Terrane, Araklı-Trabzon, NE Turkey. Geological Journal 40: 425-440.

Zheng YF, Hoefs J (1993). Carbon and oxygen isotopic covariations in hydrothermal calcite: Theoretical modeling on mixing processes and application to Pb-Zn deposits in the Harz Mountains, Germany. Mineralium Deposita 28 (2): 79-89.

Supplementary data

Table S1. Semiquantitative mineralogical composition of clay fraction in the dacite-I and dacite-II samples.

Sample	Rock type	Mineral assemblages	Semiquantitative mineralogical composition (%)
Dacite-I			
25	Dacitic tuff	Illite + smectite + quartz + feldspar ± chlorite	45 I + 41 S + 7 Qz + 7 Fs
164	Dacitic tuff	Illite + quartz + feldspar	96 I + 2 Qz + 2 Fs
A1	Agglomerate	Chlorite + illite + feldspar + quartz	74 Chl + 13 I + 10 Fs + 3 Qz
A2	Agglomerate	Chlorite + illite + quartz + feldspar	52 Chl + 43 I + 3 Qz + 2 Fs
A3	Agglomerate	Illite + chlorite + feldspar + quartz	62 I + 23 Chl + 8 Fs + 7 Qz
A4	Agglomerate	Illite + chlorite + feldspar + quartz	54 I + 38 Chl + 4 Fs + 4 Qz
A6	Agglomerate	Chlorite + illite + quartz + feldspar	63 Chl + 32 I + 3 Qz + 2 Fs
A7	Agglomerate	Chlorite + illite + feldspar + quartz	78 Chl + 15 I + 5 Fs + 2 Qz
A8	Agglomerate	Chlorite + illite + feldspar + quartz	49 Chl + 36 I + 9 Fs + 6 Qz
D1	Agglomerate	Illite + quartz ± smectite	89 I + 11 Qz
D2	Agglomerate	Illite + quartz	84 I + 16 Qz
D4	Agglomerate	Illite + kaolinite + quartz + feldspar ± smectite	57 I + 24 K + 14 Qz + 5 Fs
D6	Agglomerate	Illite + quartz + feldspar	78 I + 15 Qz + 7 Fs
D8	Agglomerate	Illite + kaolinite + quartz + feldspar ± smectite	79 I + 11 K + 6 Qz + 4 Fs
50	Dacite	Illite + chlorite + feldspar + quartz	62 I + 27 Chl + 8 Fs + 3 Qz
B3	Dacite	Illite + quartz + feldspar	77 I + 17 Qz + 6 Fs
B5	Dacite	Illite + quartz + feldspar	78 I + 15 Qz + 7 Fs
B6	Dacite	Illite + quartz + feldspar	87 I + 10 Qz + 3 Fs
B8	Dacite	Illite + quartz + feldspar	96 I + 2 Qz + 2 Fs
B9	Dacite	Illite + kaolinite + quartz	76 I + 14 K + 10 Qz
B11	Dacite	Illite + quartz	95 I + 5 Qz
161	Dacite	Illite + quartz + feldspar	92 I + 4 Qz + 4 Fs
232	Dacite	Kaolinite + illite + smectite +quartz + feldspar	9 K + 36 I + 11 S + 2 Qz + 2 Fs
241	Dacite	Illite + kaolinite + feldspar + quartz	81 I + 12 K + 4 Fs + 3 Qz
260	Dacite	Chlorite + illite + feldspar + quartz	66 Chl + 28 I + 5 Fs + 1 Qz
288	Dacite	Illite + feldspar + quartz	97 I + 2 Fs + 1 Qz
528	Dacite	Illite + quartz + feldspar	94 I + 3 Qz + 3 Fs
448	Dacite	Illite + kaolinite + feldspar + quartz	76 I + 19 K + 3 Fs + 2 Qz
560	Dacite	Illite + kaolinite + feldspar + quartz	65 I + 31 K + 2 Fs + 2 Qz
Dacite-II			
65b	Dacitic tuff	Illite + quartz	88 I + 12 Qz
496	Dacitic tuff	Illite + quartz + feldspar	96 I + 2 Qz + 2 Fs
X3	Dacitic tuff	Illite + quartz	97 I + 3 Qz
118	Agglomerate	Illite + feldspar + quartz	79 I + 8 Fs + 3 Qz
131c	Dacite	Illite + kaolinite + feldspar + quartz	59 I + 34 K + 5 Fs + 2 Qz
131d	Dacite	Illite + kaolinite + feldspar + quartz	56 I + 37 K + 5 Fs + 2 Qz
142	Dacite	Illite + kaolinite + feldspar + quartz	67 I + 26 K + 5 Fs + 2 Qz
301	Dacite	Illite + chlorite + quartz + feldspar	62 I + 34 Chl + 2 Qz + 2 Fs
382	Dacite	Illite + quartz + feldspar	90 I + 6 Qz + 4 Fs
396a	Dacite	Illite + quartz + feldspar	95 I + 3 Qz + 2 Fs

Table S1. (Continued).

397	Dacite	Illite + quartz + feldspar	90 I + 6 Fs + 4 Qz
359	Dacite	Illite + kaolinite + quartz	68 I + 29 K + 3 Qz
388	Dacite	Illite+quartz+feldspar	90 I + 6 Qz + 4 Fs
431	Dacite	Illite + chlorite + smectite + quartz + feldspar	61 I + 29 Chl + 8 S + 1 Qz + 1 Fs
492	Dacite	Illite + quartz + feldspar	92 I + 4 Qz + 4 Fs
494	Dacite	Illite + quartz + feldspar	92 I + 4 Qz + 4 Fs
495	Dacite	Illite + kaolinite + quartz + feldspar	61 I + 30 K + 5 Fs + 4 Qz
495a	Dacite	Kaolinite + illite + quartz	81 K + 17 I + 2 Qz
499	Dacite	Kaolinite + chlorite + illite + quartz	37 K + 35 Chl + 26 I + 2 Qz
512	Dacite	Illite + quartz + feldspar	96 I + 2 Qz + 2 Fs
I: Illite; Chl: Chlorite; K: Kaolinite; S: Smectite; Qz: Quartz; Fs: Feldspar.			

Table S2. Mineral compositions calculated using the MINSQ method from whole-rock major element analyses for dacite-I and dacite-II samples (wt%; n = 19).

Mineral/ sample	50	255	528	260	288	25	161	260	164	T	X1	232	246	275	304	448	560	565	247
Quartz	19.7	46.3	36.9	20.3	20.8	35.6	25.2	16.7	37.6	43.5	37.5	22.1	24.8	15.4	26.6	43.9	13.3	22.5	33.9
K-feldspar	16.0	15.8	11.6	9.80	15.2	8.50	19.4	7.80	0.00	0.00	0.00	8.20	2.70	0.00	4.80	14.3	16.8	13.2	13.7
Albite	28.0	18.8	33.5	0.00	0.00	18.7	14.6	0.00	0.00	0.00	0.00	0.00	0.00	0.00	0.00	0.00	0.00	0.00	0.00
Oligoclase	0.00	0.00	0.00	32.0	16.0	0.00	0.00	28.8	28.1	23.6	0.00	10.7	23.0	27.1	31.4	16.5	17.7	24.9	11.7
Hornblende	0.00	0.00	0.00	0.00	0.00	0.00	0.00	0.00	0.00	0.00	6.40	0.00	13.7	0.00	0.00	0.00	0.00	0.00	0.00
Fe-chlorite	0.00	0.00	0.00	6.40	0.00	1.20	1.50	5.50	1.30	5.80	2.90	0.00	0.00	0.00	0.00	0.00	0.00	0.00	0.00
Mg-chlorite	4.70	2.50	0.00	0.00	0.00	0.80	0.10	0.30	0.00	0.00	0.00	0.00	0.00	10.5	10.7	2.30	0.00	8.80	0.00
Illite	23.3	0.00	7.10	8.50	13.1	9.20	5.70	15.8	25.7	21.7	26.6	13.4	20.0	20.4	12.7	7.00	14.1	9.50	14.8
Pyrophyllite	6.80	14.5	8.70	11.1	19.2	0.00	23.2	9.50	3.40	0.00	23.5	0.00	0.00	0.00	6.90	0.00	16.2	0.00	0.00
Kaolinite	0.00	0.00	0.00	0.00	0.00	18.6	0.00	0.00	0.00	0.00	0.00	29.0	9.30	13.1	0.00	8.20	8.40	11.4	16.5
Smectite	0.00	0.00	0.00	0.00	0.00	5.20	7.40	0.00	0.00	0.00	0.00	0.00	0.00	0.00	0.00	0.00	0.00	0.00	0.00
Calcite	0.00	0.60	0.00	0.00	6.20	0.00	0.80	2.10	0.00	0.00	2.60	5.10	0.30	0.00	0.00	1.60	3.00	2.10	1.50
Ankerite	1.00	0.00	0.00	4.30	0.00	0.20	1.50	3.30	0.00	2.60	0.00	9.40	0.00	6.10	3.30	0.00	3.70	0.00	5.80
Siderite	0.00	0.00	0.10	0.00	0.00	0.00	0.00	0.00	0.00	0.00	0.00	0.00	0.00	0.00	0.00	0.00	0.00	0.00	0.00
Pyrite	0.00	0.00	0.00	0.00	0.10	0.60	0.20	0.10	0.00	0.30	0.00	0.20	1.90	0.20	0.10	0.00	0.80	0.50	0.10
Biotite	0.00	0.00	0.00	0.00	4.70	0.00	0.00	0.00	0.00	0.00	0.00	0.00	0.00	0.00	0.00	0.00	0.00	0.00	0.00
Epidote	0.00	0.00	0.00	7.60	1.70	0.00	0.00	8.90	0.00	0.00	0.00	0.00	0.00	0.00	0.00	5.20	2.30	0.00	0.00
Apatite	0.00	0.00	0.00	0.00	0.00	0.00	0.00	0.00	0.80	0.00	0.00	0.00	0.00	0.00	0.00	0.00	0.00	0.00	0.00
Rutile	0.00	0.00	0.00	0.00	0.00	0.00	0.20	0.30	0.00	0.40	0.00	0.20	0.20	0.40	0.20	0.10	0.20	0.70	0.00
Hematite	0.60	1.50	2.00	0.00	1.90	0.30	0.20	0.60	1.40	1.10	0.60	0.70	4.10	2.20	1.40	1.00	1.00	3.40	0.40
Total	100.2	100.0	99.9	100.0	98.9	98.9	100.0	99.7	98.3	99.0	100.1	98.8	100.0	95.4	98.1	100.1	97.5	97.0	98.4
Residual (r^2)	0.10	0.30	0.20	0.00	0.00	0.00	0.00	0.00	1.00	0.00	0.70	0.10	0.10	0.00	0.00	0.00	0.00	0.10	0.00

Table S2. Continued (wt%; n= 17).

Mineral/sample	431	285	86	131	142	301	311	388	397	494	496	512	G1	359	382	492	419
Quartz	40.9	37.8	22.8	30.9	28.7	27.5	31.0	36.4	36.1	35.4	33.1	43.9	39.1	25.9	23.2	30.8	24.5
K-feldspar	10.9	1.80	3.20	10.3	12.1	1.80	2.20	6.90	9.50	0.40	5.80	8.50	24.6	19.4	21.6	23.2	15.8
Albite	17.7	0.00	0.00	0.00	0.00	0.00	0.00	0.00	0.00	0.00	0.00	0.00	0.00	0.00	0.00	0.00	0.00
Oligoclase	0.00	12.2	25.3	15.8	24.5	12.3	17.2	19.5	22.8	5.10	13.6	11.4	20.1	6.30	3.50	0.00	6.10
Hornblende	0.00	0.00	0.00	0.00	0.00	1.30	0.90	0.00	0.10	0.00	0.00	0.00	0.00	0.00	0.00	0.20	0.00
Muscovite	0.00	2.90	0.00	0.00	0.00	20.9	22.1	0.00	14.9	0.00	24.3	0.00	0.00	0.00	0.00	0.00	0.00
Fe-chlorite	0.00	0.00	0.00	0.00	0.00	3.60	1.30	0.00	1.50	0.00	1.40	0.00	0.00	0.00	0.00	0.20	0.00
Mg-chlorite	0.00	0.00	4.90	0.00	2.20	7.40	6.10	0.00	0.00	11.2	0.00	0.00	0.00	0.00	0.00	2.30	8.10
Illite	24.6	37.9	34.6	21.9	12.4	10.4	11.6	26.8	12.0	31.9	19.9	23.6	6.10	15.4	16.6	11.5	33.9
Pyrophyllite	4.90	0.00	0.00	15.0	12.6	0.00	0.00	7.10	0.00	0.00	0.00	3.40	0.40	23.6	31.0	30.1	0.00
Kaolinite	0.00	0.00	0.00	0.00	0.00	0.00	0.00	0.00	0.00	0.00	0.00	0.00	7.80	4.30	2.10	0.00	0.00
Calcite	0.10	4.40	5.10	1.50	4.20	6.80	4.10	0.00	0.20	2.40	0.20	2.00	0.00	0.00	0.00	0.20	3.30
Ankerite	0.00	0.00	1.10	2.20	0.00	0.40	0.80	0.00	0.00	0.00	0.20	0.00	0.00	0.00	0.10	0.00	4.90
Pyrite	0.00	0.00	0.00	0.00	0.20	0.10	0.10	0.30	0.40	0.00	0.10	0.00	0.10	0.70	0.10	0.10	0.20
Epidote	0.00	0.00	0.00	0.00	0.00	0.00	0.00	0.00	0.00	12.8	0.00	7.10	0.00	0.00	0.00	0.00	0.00
Rutile	0.00	0.00	0.10	0.10	0.20	0.30	0.30	0.10	0.10	0.30	0.30	0.10	0.10	0.10	0.10	0.30	0.00
Hematite	1.00	3.00	3.00	2.10	2.70	0.60	1.50	0.90	0.20	0.70	0.00	0.00	0.90	1.30	0.80	0.00	0.00
Total	100.1	100.0	100.1	99.8	99.8	93.4	99.2	98.0	97.8	100.2	98.9	100.0	99.2	97.0	99.1	98.9	96.8
Residual (r^2)	0.30	0.40	0.70	0.30	0.20	0.00	0.00	0.30	0.00	0.20	0.00	0.20	0.30	0.00	0.00	0.00	0.30